

2 **Using hydrologic landscape classification and climatic time series**  
3 **to assess hydrologic vulnerability of the Western U.S. to climate**

4 Chas E. Jones Jr.<sup>1\*</sup>, Scott G. Leibowitz<sup>2</sup>, Keith A. Sawicz<sup>3</sup>, Randy L. Comeleo<sup>2</sup>, Laurel E.  
5 Stratton<sup>4</sup>, Philip E. Morefield<sup>5</sup>, Christopher P. Weaver<sup>6</sup>

6 <sup>1</sup> Oak Ridge Institute for Science and Education (ORISE), c/o U.S. Environmental Protection Agency, Center for  
7 Public Health and Environmental Assessment, Pacific Ecological Systems Division, 200 SW 35th St., Corvallis, OR  
8 97333, USA; Current affiliation: Affiliated Tribes of Northwest Indians, Corvallis, OR 97333, USA  
9

10 <sup>2</sup> U.S. Environmental Protection Agency, Center for Public Health and Environmental Assessment, Pacific Ecological  
11 Systems Division, 200 SW 35th St., Corvallis, OR 97333, USA  
12

13 <sup>3</sup> Oak Ridge Institute for Science and Education (ORISE), c/o U.S. Environmental Protection Agency, Center for  
14 Public Health and Environmental Assessment, Pacific Ecological Systems Division, 200 SW 35th St., Corvallis, OR  
15 97333, USA; Current Affiliation: AIR Worldwide, 131 Dartmouth Street #4, Boston, MA 02116, USA  
16

17 <sup>4</sup> c/o U.S. Environmental Protection Agency, Center for Public Health and Environmental Assessment, Pacific  
18 Ecological Systems Division, 200 SW 35th St., Corvallis, OR 97333, USA  
19

20 <sup>5</sup> U.S. Environmental Protection Agency, Center for Public Health and Environmental Assessment, Health and  
21 Environmental Effects Assessment Division, Washington, DC 20460, USA  
22

23 <sup>6</sup> U.S. Environmental Protection Agency, Center for Public Health and Environmental Assessment, Health and  
24 Environmental Effects Assessment Division, Research Triangle Park, NC 27709, USA

25 *Correspondence to:* Chas E. Jones Jr. (chas@chasjones.com)

26 **Abstract.** We apply the hydrologic landscapes (HL) concept to assess the hydrologic vulnerability of the western  
27 United States (U.S.) to projected climate conditions. Our goal is to understand the potential impacts of hydrologic  
28 vulnerability for stakeholder-defined interests across large geographic areas. The basic assumption of the HL approach  
29 is that catchments that share similar physical and climatic characteristics are expected to have similar hydrologic  
30 characteristics. We use the Hydrologic Landscape vulnerability approach (HLVA) to map the HLVA index (an  
31 assessment of climate vulnerability) by integrating hydrologic landscapes into a retrospective analysis of historical  
32 data to assess variability in future climate projections and hydrology, which includes temperature, precipitation,  
33 potential evapotranspiration, snow accumulation, climatic moisture, surplus water, and seasonality of water surplus.  
34 Projections that are beyond two-standard deviations of the historical decadal average contribute to the HLVA index  
35 for each metric. Separating vulnerability into these seven separate metrics allows stakeholders and/or water resource  
36 managers to have a more specific understanding of the potential impacts of future conditions. We also apply this  
37 approach to examine case studies. The case studies (Mt. Hood, Willamette Valley, and Napa-Sonoma Valley) are  
38 important to the ski and wine industries and illustrate how our approach might be used by specific stakeholders. The  
39 resulting vulnerability maps show that temperature and potential evapotranspiration are consistently projected to have  
40 high vulnerability indices for the western U.S. Precipitation vulnerability is not as spatially uniform as temperature.  
41 The highest elevation areas with snow are projected to experience significant changes in snow accumulation. The  
42 seasonality vulnerability map shows that specific mountainous areas in the West are most prone to changes in  
43 seasonality, whereas many transitional terrains are moderately susceptible. This paper illustrates how HL and the  
44 HLVA can help assess climatic and hydrologic vulnerability across large spatial scales. By combining the HL concept  
45 and HLVA, resource managers could consider future climate conditions in their decisions about managing important  
46 economic and conservation resources.

## 47 **1 Introduction**

48 A stable and predictable water supply is imperative for food security, ecosystem sustainability, economic stability,  
49 and even national security (National Intelligence Council, 2012), and is related to the threats of increased flooding,  
50 droughts, wildfire, and more extreme temperatures (Mancosu et al., 2015; Mekonnen and Hoekstra, 2016). The  
51 recognition of the potential socio-ecological threats of climate change on the water supply is a critically important  
52 topic, and the development of planning tools that identify vulnerabilities to these systems could help decision-makers  
53 assess the risks of environmental changes imposed by climate as well as other contemporary risks (e.g., population  
54 growth and habitat conversion) (Glick et al., 2011; Lawler et al., 2010). Climatic and hydrologic change will not  
55 impact stakeholders equally across sectors, thus the specific concerns and adaptation strategies of different industries  
56 threatened by those risks will vary. The hydrologic landscapes vulnerability assessment described herein provides a  
57 relatively simple approach for assessing hydrologic vulnerability based upon inferences of hydrologic behavior (using  
58 hydrologic landscapes) in response to climatic impacts. This approach can be applied across large geographic regions  
59 and can potentially benefit numerous sectors, including environmental, economic, and other ecosystem services.

60 Numerous studies have examined projected changes in climate and hydrology on regional and national scales that  
61 relate to this study in the western United States (U.S.). Climate-related risk to snow-dominated areas and ski areas  
62 were identified by Nolin and Daly (2006) in the Pacific Northwest (PNW, which includes Washington, Oregon, and  
63 Idaho), whereas observations and modeled simulations for snow water equivalents (SWE) were found to be similar in  
64 the western U.S. (Mote et al. 2005). Barnett et al. (2005) found potential climate-driven water supply deficits in snow-  
65 dominated areas around the globe. McAfee (2013) examined projected changes in potential evapotranspiration (PET,  
66 calculated using numerous methods) and found regional analyses to be more inconsistent than studies across the  
67 conterminous U.S., which indicated sensitivities to the methods used. Hill et al. (2013, 2014) predicted thermal  
68 vulnerability of streams and river ecosystems to climate across the U.S., while Battin et al. (2007) found that salmon  
69 habitat in snow-dominated streams was more vulnerable than habitat in lowland streams. The relevant analyses of  
70 Nijssen et al. (2001) on hydrologic sensitivity of rivers globally found: 1) ubiquitous warming, with greatest warming  
71 in winter months at higher latitudes, 2) more precipitation with high variability, 3) early to mid-spring snowmelt  
72 caused increased spring streamflow peak in coldest basins, decreased spring runoff and increased winter runoff in  
73 transitional basins, and 4) increased annual streamflow with high latitude basins. While snow-fed streams in the  
74 western US seem less likely to change flow regimes, perennial and intermittent, rain-fed streams are more likely to  
75 change in flow regime (Dhungle et al., 2016). In response to droughts of the recent past, Mann and Gleick (2015)  
76 highlight the strong correlation between very hot years and very dry years; thus as temperatures increase at the upper  
77 extreme, precipitation is becoming more scarce. A study by Cook et al. (2015) found a growing risk of unprecedented  
78 drought in the western U.S. based on temperature projections and no clear pattern in future precipitation. This sampling  
79 of the existing research highlights the cross-cutting hydrological changes that are occurring across the nation and  
80 illustrates how different sectors and geographies are experiencing different impacts,

81 “Vulnerability” has been defined in many ways, depending upon discipline and application (Adger, 2006; Füssel,  
82 2007). Vulnerability assessments often integrate exposure, sensitivity, and adaptive capacity to stressors (Adger, 2006;  
83 Füssel, 2007; Füssel and Klein, 2006; IPCC, 2014). Researchers have studied vulnerability at varying scales across  
84 numerous regions for a diversity of stakeholders, and they tend to focus on the most relevant metrics for their particular  
85 application (Farley et al., 2011; Glick et al., 2011; IPCC, 2014; Nolin and Daly, 2006; U.S. Global Change Research  
86 Program, 2011; Watson et al., 2013). Yet, better products and services are needed to enable local communities to plan  
87 for and respond to hydrologic change, which includes services that improve understanding, observing, forecasting,  
88 and warning about significant hydrologic events (Tansel, 2013). Glick et al. (2011) and Lawler et al. (2010) both  
89 emphasize the importance to managers of understanding the potential impacts of climate on the resources that they  
90 manage.

91 There have been many efforts to assess hydrologic vulnerability related to specific stakeholders, ecosystems, or  
92 locations. For example, Vörösmarty et al. (2000) examined the vulnerability of global water resources to changes in  
93 climate and population growth. Hill et al. (2014) assessed stream temperature vulnerability to climate for sites across

94 the U.S. In another example, Winter (2000) suggested that the vulnerability of wetlands to changes in climate  
95 depended upon their position within the hydrologic landscape.

96 There are opportunities to build upon previous efforts to map hydrologic vulnerability across large geographic areas,  
97 while creating tools that stakeholders may use to understand the potential impacts for their asset of interest in specific  
98 watersheds. Winter (2001) described the concept of classifying the physical landscape and climatic properties of large  
99 landscape units based on hydrologic landscapes (HL). Surface and ground water availability in watersheds is impacted  
100 by differences in geology, terrain, soils, seasonal temperature patterns, precipitation magnitude, and precipitation  
101 timing (Tague et al., 2013; Winter, 2001) and are not uniform across regions (Hamlet, 2011; Jung and Chang, 2012;  
102 Tague and Grant, 2004). Catchments that share similar key physical and climatic characteristics are expected to have  
103 similar hydrologic characteristics; i.e., surface and ground water interactions, deposition, timing, and accumulation of  
104 precipitation, surface runoff patterns, and groundwater flow (Nolin, 2011; Thompson and Wallace, 2001).

105 The HL concept has been applied to the U.S. using a clustering method (Wolock et al., 2004) to develop twenty non-  
106 contiguous regions, which were much larger than the catchment scale. Since that effort, modified approaches have not  
107 used clustering approaches, but have used catchment-based classification in Oregon (Leibowitz et al., 2014; Patil et  
108 al., 2014; Wigington et al., 2013), Nevada (Maurer et al., 2004), the PNW (Comeleo et al., 2014; Leibowitz et al.,  
109 2016), and Bristol Bay, Alaska (Todd et al., 2017). In applying the HL approach in Oregon and the PNW, the clustering  
110 approach was abandoned for a conceptual approach based upon important factors known to contribute to hydrologic  
111 flow (Wigington et al., 2013), where two climatic factors and three landscape characteristics were categorized for each  
112 catchment; the resulting classification allows the estimation of catchment-scale hydrologic behavior across large  
113 spatial scales. The approach shows promise in predicting seasonal and monthly hydrologic patterns (Leibowitz et al.,  
114 2014). Leibowitz et al. (2014) adapted the classification system applied by Wigington et al. (2013) to illustrate the  
115 applicability of HLs at the watershed scale for representing normal (1971-2000) monthly average streamflow in three  
116 case study watersheds in Oregon. They used climate projections (2041-2070) to estimate hydrologic behavior of  
117 watersheds relative to 1971-2000. Leibowitz et al. (2016) expanded the approach and applied the HL classification to  
118 Oregon, Washington, and Idaho. The more recent studies using the hydrologic landscape classification approach have  
119 been applied at a watershed scale (Patil et al. 2014, Leibowitz et al. 2016, Todd et al. 2017).

120 A number of tactics have been used to investigate the influence of climate on hydrologic behavior (Luce and Holden,  
121 2009; Safeeq et al., 2014; Vano et al., 2015). To extend the work previously completed from HL-based climate  
122 projections, we assess hydrologic vulnerability at the catchment scale by integrating the HL approach into an analysis  
123 of climatic variability. Our hydrologic landscape vulnerability approach (HLVA) provides spatially continuous,  
124 application-specific estimates of climatic vulnerability (maps of the HLVA indices). One of the benefits of the HLVA  
125 is to place recent and projected environmental changes in the context of available historic data. In the HLVA, we use  
126 proxies for the three components of vulnerability: a) historic climate data and their derivatives as proxies for sensitivity  
127 (the sensitivity of a particular system to each variable); b) climate projections as proxies for exposure (the future  
128 projected condition increases or decreases a system's exposure to a change); and c) qualitative considerations of

129 ecosystems, stakeholders, or industries as proxies for adaptive capacity (the presence of a system in a location is  
130 indicative that the system has historically had sufficient adaptive capacity to exist in that area). Using HLVA, we  
131 examine vulnerability to changes in temperature, precipitation, potential evapotranspiration, snow accumulation,  
132 surplus water, climatic moisture, and seasonality of the water surplus. This method highlights areas that are projected  
133 to experience deviations from historic conditions to understand the patterns in magnitude, timing, and type of  
134 precipitation and the quantity and seasonality of available water at a catchment scale. These estimates of hydrologic  
135 vulnerability could offer important insight into the potential resilience of socially and economically valuable locations  
136 and stakeholders in an area.

137 We assess the hydrologic vulnerability of socially and economically valuable locations by applying the HL concept  
138 using climatic projections in the western U.S. We analyzed the output from the HL analyses to address three research  
139 objectives: 1) develop an index of vulnerability based on climate; 2) map areas that are projected to be more vulnerable  
140 to environmental change; and 3) determine the vulnerability indices for socially and economically valuable locations,  
141 including three example case studies for regional industries that are economically important in the region. By  
142 integrating the concept of hydrologic landscape classification, hydrologic vulnerability, and climatic impacts, this  
143 study lays the groundwork for making spatially explicit generalizations about the hydrologic vulnerability of socially  
144 and economically valuable locations across large landscapes.

## 145 **2 Methods**

### 146 **2.1 Study Area**

147 The study area includes the states of Washington, Oregon, Idaho, California, Nevada, and Arizona in the western U.S.  
148 (Fig. 1). These states extend across a wide range of climates and diverse physiographic settings. The lowest elevation  
149 across the six states is 85 m below sea level (Death Valley, California), while the highest elevation is 4421 m above  
150 sea level (Mt. Whitney, California) [U.S.G.S. National Elevation Dataset available at:  
151 <https://nationalmap.gov/elevation.html>]. The Sierra-Nevada Mountains are oriented in a north-south direction near the  
152 eastern border of California and transition to the Cascade mountain range that is oriented north-south through Oregon  
153 and Washington (US Topo Quadrangles available at: <https://nationalmap.gov/ustopo>). There are numerous other  
154 mountain ranges in the other states as well. The Sierra-Nevada and Cascade mountain ranges generate orographic  
155 effects that cause upwind areas to the west to have greater precipitation relative to the downwind, eastern regions  
156 (Dettinger et al., 2004; Siler et al., 2013). High elevation areas receive most of their precipitation as snow (Brekke et  
157 al., 2009; Mote et al., 2005), while lowland and coastal areas receive predominantly rain (Brekke et al., 2009; Mock,  
158 1996), but much of the study area receives a balance of snow and rain. The topographic differences drive precipitation  
159 patterns across the area and cause differences in the total annual precipitation or the seasonality of maximum  
160 precipitation (Mock, 1996). In the arid southwest, summer monsoons deliver most of the annual precipitation, whereas  
161 in the PNW, winter rains and snows prevail (Mock, 1996). However, the western U.S. is regularly affected by  
162 atmospheric rivers that deliver large quantities of rain or snow over short periods (Dettinger, 2011; Hidalgo et al.,

163 2009). The seasonal variability of surface air temperature varies widely across the study area. Portions of each state  
164 are classified as deserts with summer maximum temperatures regularly exceeding 40°C (NOAA State Climate  
165 Extremes Committee, 2016). Each state has also recorded temperatures less than -40°C (NOAA State Climate  
166 Extremes Committee, 2016). Some areas have mild climates with little seasonal variation in temperature (Daly,  
167 2016b). Geology in the study area varies from high permeability sedimentary deposits or relatively recent volcanic  
168 deposits, to low permeability igneous metamorphic and sedimentary formations and older volcanics (Comeleo et al.,  
169 2014; Stratton et al., 2016).

## 170 **2.2 Hydrologic landscape classification**

171 Assessment units (AUs) are aggregations of NHDPlusV2 catchments (McKay et al., 2012) that were grouped to have  
172 a target area of 80 km<sup>2</sup>, as described in Leibowitz et al. (2016). In this study, the same assessment units used in the  
173 Leibowitz et al. 2016 study have been used and their method applied to the expanded six state study region to delineate  
174 29,097 assessment units for the study's expanded 6 state study region. For this analysis, we retain an AU if its centroid  
175 was located within the boundary of our project area or if the AU extended across an international boundary. All AU  
176 polygons are clipped to the international boundary of the U.S. These conditions allow us to avoid edge effects at  
177 international and state borders by avoiding overlapping AUs at state boundaries and analyzing the HLs up to all  
178 international borders.

179 Building upon Winter's (2001) approach and the Wolock et al. (2004) clustering approach, Wigington et al. (2013)  
180 developed their simple conceptual HL classification based on climatic and physical characteristics of the physical  
181 watershed. They combined five indices related to hydrologic flow (Fig. 2a) to characterize the major drivers that  
182 control the magnitude and timing of water movement through the landscape and into the groundwater or stream  
183 network: (1) climate, which describes the overall water availability, (2) seasonality of water surplus, which is the  
184 season when the maximum excess of water is available to infiltrate into the soil or flow as surficial runoff, (3)  
185 subsurface permeability, (4) terrain, and (5) surface permeability. Note that Wigington et al. (2013) referred to  
186 subsurface and surface permeability as aquifer and soil permeability, respectively. The five HL indices, described in  
187 more detail below (Sections 2.2.1 through 2.2.5), are concatenated into a 5-character HL code (e.g., WsLMH, SwHTh,  
188 or DfHfL) that characterizes an AU.

189 Leibowitz et al. (2016) modified the Wigington et al. (2013) approach by including: the use of assessment units based  
190 on National Hydrography Dataset Plus V2 catchments, a modified snowmelt model that was validated over a broader  
191 area, a subsurface permeability index that does not require pre-existing aquifer permeability maps, and a surface  
192 permeability threshold based on objective criteria. Using this modified method (herein described as the modified  
193 Wigington et al. (2013) approach), they developed an HL map of the PNW. Here, we used the modified Wigington et  
194 al. (2013) approach to develop an HL classification of California, Nevada, and Arizona. This was then combined with  
195 the PNW map (Leibowitz et al., 2016) to create an HL map of the study area.

### 196 **2.2.1 Climate**

197 The Wigington et al. (2013) approach derived the climate index from the Feddema Moisture Index (FMI) (Feddema,  
198 2005):

$$199 \quad FMI = \begin{cases} 1 - \frac{PET}{P} & \text{if } P \geq PET \\ \frac{P}{PET} - 1 & \text{if } P < PET \end{cases} \quad (1)$$

200 where FMI (Eq. (1)) values range from -1.0 (arid) to 1.0 (very wet). P is the mean precipitation (mm) over a 30-year  
201 period, which is derived from climate data described in Section 2.3, and PET is the potential evapotranspiration (mm)  
202 calculated using the Hamon (1961) method, that utilizes mean daily temperature, daytime length (calculated based on  
203 latitude), and a calibration coefficient. The range of FMI values was the basis for defining a climate index consisting  
204 of six classes: arid (A;  $-1.0 \leq FMI < -0.66$ ), semiarid (S;  $-0.66 \leq FMI < -0.33$ ), dry (D;  $-0.33 \leq FMI < 0.0$ ), moist (M;  
205  $0.0 \leq FMI < 0.33$ ), wet (W;  $0.33 \leq FMI < 0.66$ ), and very wet (V;  $0.66 \leq FMI < 1.0$ ) (Wigington et al., 2013). FMI  
206 was calculated using regional precipitation and temperature rasters (described in Section 2.3) for each period of  
207 interest. The FMI value was then averaged over each AU.

### 208 2.2.2 Seasonality

209 We used the Leibowitz et al. (2016) approach to develop a seasonality index that identifies the season of the maximum  
210 monthly average snowpack-corrected surplus water ( $S'_m$ ):

$$211 \quad S'_m = S_m - \Delta PACK_m^*$$

$$212 \quad S'_m = (P_m - PET_m) - (PACK_m^* - PACK_{m-1}^*) \quad (2)$$

213 where  $S'_m$  (Eq. (2)) is the average snowpack-corrected water surplus (mm) for month  $m$ ,  $S_m$  is monthly water surplus  
214 ( $P - PET$ ), and  $P_m$  and  $PET_m$  are monthly precipitation and monthly PET, respectively.  $PACK_m^*$  is a monthly bias-  
215 corrected snowpack value (in mm of snow water equivalent, or SWE) restricted to values greater than zero, based on  
216 the Leibowitz et al. (2016) modifications to the Leibowitz et al. (2012) snowpack model. Note that  $\Delta PACK_m^*$  can have  
217 negative values, which represents snow melt. For each month,  $S'_m$  was calculated for the regional raster, before  
218 identifying the month of maximum  $S'_m$  for the majority of pixels in each AU. The month of maximum  $S'_m$  was used  
219 to identify the season of maximum  $S'_m$  based upon four seasonality classes: fall (f; October–December), winter (w;  
220 January–March), spring (s; April–June), and summer (u; July–September). The PNW analysis by Leibowitz et al.  
221 (2016) only included two seasonality classes; summer seasonality did not occur, while fall and winter were combined  
222 into a winter class, since this represented the PNW's wet season. For this analysis, winter and fall were separated and  
223 all four seasonality classes were used, because fall and winter are distinct seasons in other parts of the nation.

### 224 2.2.3 Subsurface permeability

225 Leibowitz et al. (2016) utilized the Comeleo (2014) aquifer permeability dataset. We applied a similar approach to the  
226 Stratton et al. (2016) aquifer permeability datasets, which is herein referred to as subsurface permeability. Each dataset

227 classifies the subsurface permeability into high (H) and low permeability (L) classes, which are assigned with a  
228 threshold of  $8.5 \times 10^{-2} \text{ m day}^{-1}$  hydraulic conductivity. Using these data, we analyzed the subsurface permeability of  
229 each AU by identifying the subsurface permeability class for the majority of pixels within each AU in California,  
230 Nevada, and Arizona.

#### 231 **2.2.4 Terrain**

232 To classify terrain, we used the same approach as Wigington et al. (2013). We analyzed a 30 m Digital Elevation  
233 Model to classify the landscape based upon the topographic characteristics of each AU. “Mountainous” (M) areas had  
234 AUs with <10 % of the area identified as flat (< 1 % slope) and greater than 300 m of total relief. AUs with more than  
235 50 % area having < 1 % slope were classified as “flat” (F). All other AUs were identified as “transitional” (T).

#### 236 **2.2.5 Surface permeability**

237 For surface permeability, the Leibowitz et al. (2016) HL approach utilized the STATSGO soil permeability raster  
238 developed by Pennsylvania State University Center for Environmental Informatics ([www.cei.psu.edu](http://www.cei.psu.edu)) for the top 10  
239 cm of soil (Miller and White, 1998) in the conterminous U.S. The STATSGO soils database was selected because of  
240 its complete coverage of the conterminous U.S., despite SSURGO’s higher spatial resolution, yet incomplete coverage  
241 of the study area. Leibowitz et al. (2016) identified whether the majority of each AU had high (H;  $>1.52 \text{ cm h}^{-1}$ ) or  
242 low (L;  $\leq 1.52 \text{ cm h}^{-1}$ ) soil permeability. We applied the same approach to classify surface permeability of each AU  
243 into two classes throughout the region.

### 244 **2.3 Climate analyses**

#### 245 **2.3.1 Climate normal (1971–2000)**

246 The climate normal was defined as the 1971-2000 period to align with the Leibowitz et al. (2016) study. Average  
247 monthly precipitation and mean temperature were acquired from Parameter-elevation Regressions on Independent  
248 Slopes Model (PRISM; Daly, 2016b) data for our normal climatic period at a resolution of approximately 400 m. The  
249 PRISM Climate Mapping Program is an ongoing effort to produce detailed, spatial climate datasets (Daly, 2016a;  
250 Daly et al., 2000). PRISM uses point measurements of climate data and a digital elevation model to map climate across  
251 the U.S. from 1895–present, including regions impacted by high mountains, rain shadows, temperature inversions,  
252 coastal regions, and associated complex meso-scale climate processes. Using ArcGIS (ESRI, 2016), the data were  
253 clipped to the project boundary and used to calculate the average for seven metrics: monthly temperature ( $^{\circ}\text{C}$ ),  
254 precipitation (mm), PET (mm), surplus water (mm), snow water equivalent (mm), the FMI climate index (unitless),  
255 and seasonality of water surplus (unitless). Each metric is an input to or products of the HL classification process.

#### 256 **2.3.2 Historical climate analyses (1901–2010)**

257 Unlike the 1971-2000 monthly precipitation and temperature data, a time series of gridded monthly historical climate  
258 data at a spatial resolution of 400 m was not available without paying a fee. However, daily PRISM data were freely  
259 available at 4 km resolution, so we used these to develop the historical climate analyses for the 1901–2010 period.  
260 These gridded data for daily mean temperature and precipitation were clipped to the project boundary and averaged



261 for each month over each decade (i.e., 1901–1910, 1911–1920, etc.). The data were then statistically downscaled to  
262 400 m using the delta method (Hijmans et al., 2005; Ramirez-Villegas and Jarvis, 2010) to match the spatial and  
263 temporal resolution of the climate normal data (using the 400 m resolution, monthly PRISM climate normal for 1971–  
264 2000 period as the high resolution dataset). We acknowledge the inaccuracies and uncertainty imposed in the  
265 temperature and precipitation datasets by applying the downscaling functions to the original climate projections. While  
266 the 400m data clearly have greater resolution and less error than the 4km data, these data were to be aggregated to  
267 assessment units with a mean area of 56 km<sup>2</sup>. In practice, the larger 4km resolution of the downscaled historical  
268 analysis should still be appropriate for the scale of the assessment units, thus the trade-offs were deemed acceptable  
269 and preferable for characterizing the hydrology and climate for these analyses with no additional budget requirements.

270 Based on the approaches described, the downscaled data were used to calculate the average monthly PET, surplus  
271 water, snow water equivalent, FMI, and seasonality of water surplus for each decade (Fig. 2b). Summary figures were  
272 generated from this data depicting spatial distribution of climate and seasonality for each decade across the project  
273 area. These data were compared to the climate normals using spatially continuous time series analyses (Fig. S1).

### 274 **2.3.3 Future climate analyses (2041–2070)**

275 In order to explore the potential range of modeled climatic response for the study area, we selected ten climate model  
276 projections from the full ensemble of World Climate Research Programme’s Coupled Model Intercomparison Project  
277 phase 5 multi-model ensemble climate dataset projections (WCRP CMIP5; <http://cmip-pcmdi.llnl.gov/cmip5>; Taylor  
278 et al., 2012). These models are based on the Representative Concentration Pathway (RCP) 8.5 emissions scenario,  
279 which assumes the highest rate of emissions into the 21<sup>st</sup> century and most closely relates to conditions observed to  
280 date (Schwalm et al., 2020). To reduce the complexity of the analyses, we used only this one emissions scenario. To  
281 select the specific model simulations to use in this study, we used the U.S. Environmental Protection Agency’s (EPA)  
282 LASSO tool ([lasso.epa.gov](http://lasso.epa.gov); U.S. EPA, 2020) to generate a scatterplot comparing future temperature and precipitation  
283 change for the different CMIP5 models over the project area. Using the scatterplot and the approach described by U.S.  
284 EPA (2020), we subjectively selected ten models that spanned the entire range of predicted climatic responses of the  
285 full ensemble in a distributed manner (Fig. 3), including drier, wetter, colder, and warmer responses. Average monthly  
286 precipitation and temperature for the ten projections (Table 1) were acquired from the monthly Bias Correction and  
287 Spatial Disaggregation (BCSD) archive (Bureau of Reclamation, 2014) for the 2041–2070 period. These data were  
288 clipped to the project boundary and resampled to a 400 m grid using a bilinear approach (ESRI ArcGIS v10.4) to  
289 match the resolution and spatial extent of the climate data. The average monthly PET, surplus water, snow water  
290 equivalent, FMI, and seasonality of water surplus were calculated from the future climate data for each assessment  
291 unit. Example figures were generated that illustrate the spatial distribution of the differences in FMI (Fig. S1 and S2)  
292 and seasonality of water surplus (Fig. S3 and S4) from the normal period for each climate projection (Fig. 2c).

### 293 **2.4 Mapping vulnerability indices**

294 As discussed in the introduction, vulnerability can be measured by assessing the *exposure*, *sensitivity*, and *adaptive*  
295 *capacity* of a system to change (Adger, 2006; Füssel, 2007; Füssel and Klein, 2006; IPCC, 2014). Hydrology and

296 climate are primary forcing factors for ecosystems (Nelson, 2005) and are critical to certain industries and stakeholders  
297 in particular areas, and thus analyses of historic variation in hydrology and climate in an area can serve as proxies for  
298 the historical *sensitivity* of those systems to environmental change. Likewise, we used future climate projections as a  
299 proxy for *exposure*. Projections that fell outside of historic observations were assumed to be associated with increased  
300 exposure to the forcing factors for environmental change, which include hydrology and climate. In terms of *adaptive*  
301 *capacity*, we assumed that the systems present in a location are adapted to the historic variability in conditions. We  
302 also assumed that the systems would become stressed by conditions far outside of those previously experienced.  
303 Further, we suggest that the greater the number of future climate projections that exceed or fall far below the historic  
304 range, the more vulnerable a system will be with respect to climate-induced changes. Thus, HLVA places projected  
305 environmental changes in the context of historic trends. The HLVA assesses vulnerability to changes in temperature,  
306 precipitation, potential evapotranspiration, surplus water, snow accumulation, climatic moisture, and seasonality of  
307 the water surplus by identifying areas that are projected to experience future deviations from historic conditions (Fig.  
308 2e).

309 The ten future climate projections (for the 2041–2070 period) were compared to the decadal averaged data from 1901–  
310 2010 for each AU. We calculated the historical standard deviation of each metric for each AU within the project area.  
311 For each metric, we assume that any projection within two-standard deviations of the historical climate values does  
312 not contribute to an increase in vulnerability, whereas projections outside of that range increase the vulnerability. We  
313 then define vulnerability for a given metric as the number of the ten projections that are outside of the historical two-  
314 standard deviation threshold. Thus, the HLVA index assesses the likelihood that a given metric will exceed a two-  
315 standard deviation threshold from the decadal mean under future climate scenarios. Because individual models exceed  
316 the threshold of two standard deviations from the mean in both the higher and lower directions, there is not a unique  
317 direction of change associated with the vulnerability index. Thus, the vulnerability index, as defined, does not convey  
318 information about projected direction of change. A vulnerability index of ten indicates that all ten climate projections  
319 were beyond two-standard deviations from the historical mean and that the area is expected to experience projected  
320 conditions that it is not adapted to. The least vulnerable areas will have an index of zero, which indicates that all future  
321 climate projections fell within the two-standard deviation threshold to which systems are adapted to. The use of  
322 standard deviations is not an appropriate threshold metric for seasonality, because it is a categorical variable. For the  
323 seasonality metric, any projected seasonality value that has not been observed decadally between 1900 and 2010  
324 increases the seasonality vulnerability index. For example, consider an AU that had predominantly experienced spring  
325 seasonality, with the occasional fall seasonality, and that 7 of 10 climate models project fall seasonality and 3 of 10  
326 models predict winter seasonality for 2041–2070. Since winter seasonality was not observed for any decade between  
327 1900 and 2010, the three predictions for winter seasonality would contribute to a vulnerability index of three for  
328 seasonality in that case. Finally, we analyzed the dominant HL code by area of the most vulnerable AUs (those having  
329 a vulnerability index greater than seven on a scale of ten) for each metric in order to gain insight about the dominant  
330 HL characteristics that relate to hydrologic vulnerability.

## 331 **2.5 Locational time series analyses**

332 Forty-five locations (Fig. 1 and Table 2) were selected for potential applications of the HL approach to demonstrate  
333 the method's relevance to potential water resource stakeholders to identify areas where we thought results could be of  
334 use to land managers. Specific sites were selected subjectively so that we could examine representative climate impacts  
335 at sites that may be of general interest. These sites include cities, national parks, mountains, national forests, and areas  
336 with hydrologically sensitive economic interests. AUs were used to represent a geographic feature if its centroid was  
337 located within the geographic boundary of a location of interest. The location boundary was defined by merging these  
338 AUs into a single polygon. For instance, the Great Basin National Park (GBNP) was covered by a single AU, rather  
339 than numerous AUs because the centroid of only one AU was within the park boundary, whereas all other AU centroids  
340 were located outside of the GBNP boundary. The time series for the decadal averages for each of the climate-related  
341 HL metrics were analyzed for the AUs associated with each location. Decadal averages were plotted at the decadal  
342 midpoint for each 10-year period from 1901 to 2010. In addition, the 1971–2000 normal average for each variable  
343 and ten climate projections (2041–2070) were also plotted. The HLVA was then used to determine the mean  
344 vulnerability index and the dominant HL code for the AUs associated with each location (Fig. 2d).

## 345 **3 Results**

### 346 **3.1 Hydrologic landscape summary**

347 Table 3 shows the percent coverage of the HL categories for the six states. Thirty percent of the region is mountainous  
348 (elevation relief of AU > 300 m and < 10 % of AU area has slope < 1 %) and 7 % is flat (AUs with more than 50 %  
349 area having < 1 % slope). The remaining area is classified as transitional. According to the soil permeability dataset  
350 (Miller and White, 1998) produced from the STATSGO soils database (Soil Survey Staff, 2016), 98 % of the surface  
351 soils (defined as the top 10 cm) are highly permeable ( $> 4.23 \mu\text{m s}^{-1}$ ). Stratton et al. (2016) and Comeleo et al. (2014)  
352 classified the subsurface permeability of the six-state region as 60 % high permeability and 40 % low permeability.  
353 During the 1971–2000 climate normal period, most of the area has the highest monthly water availability (seasonality)  
354 during the winter (63 %), followed by 24 % of the area showing fall seasonality, 13 % having spring seasonality, with  
355 only 1 % experiencing summer seasonality. In addition, 30 % of the area is classified as having a moist, wet, or very  
356 wet climate, while 70 % is dry, semi-arid or arid. The HL maps for the study area are included in the appendix (Fig.  
357 A1). HL maps for the remainder of the conterminous U.S. are also available and are included as supplemental material  
358 (Fig. S6; although subsurface permeability maps are not available for all of the lower 48 states).

### 359 **3.2 Climate Vulnerability analyses**

360 Using the analyses of historic and future climate, the vulnerability indices were mapped for all seven metrics  
361 (examples are provided for FMI and seasonality in the supplemental materials). The vulnerability maps (Fig. 4)  
362 identify areas that are subject to extreme future climatic and hydrologic variability (similar vulnerability maps for the  
363 conterminous U.S. are included in the supplemental materials (Fig. S6)). Note that while it is possible to evaluate  
364 direction of change (greater or less than two standard deviations) for the projection of an individual climate model,  
365 the vulnerability index is the integration of ten individual models. Therefore, it is possible for individual models to

366 exceed the threshold of two standard deviations from the mean in either the higher or lower directions; thus there is  
367 not a unique direction of change associated with our vulnerability index as it has been defined.

368 All climate projections indicate that temperature will change almost ubiquitously across the Pacific west, indicating  
369 uniformly high vulnerability. However, changes in precipitation are much more spatially variable. The cold deserts  
370 and Mediterranean California Ecoregions (Ecoregion level 2) have higher vulnerability, i.e., are more consistently  
371 projected to experience changes in precipitation than has been observed since 1901 on a decadal basis. In contrast,  
372 major portions of Arizona, Washington, Oregon, and California have areas with low vulnerability to change with  
373 respect to precipitation. The PET vulnerability map is similar to the temperature vulnerability map, which is not  
374 surprising since the Hamon (1961) method of calculating monthly PET uses temperature as the major input. The April  
375 1 snow accumulation (snow water equivalent) vulnerability map shows high vulnerability in many mountainous areas  
376 throughout the west. This seems to indicate that snow accumulation will change, particularly in transitional areas,  
377 compared to the most snow prone areas of the West. S' is a measure of available water (excess water available for soil  
378 infiltration or overland flow) and has less spatial uniformity of vulnerability than temperature or PET. The map for S'  
379 suggests that the Warm Desert and Marine West Coast Forest Ecoregions are more likely to experience substantial  
380 changes in available water (i.e., high vulnerability) in the future. The FMI is calculated from the ratio of PET and  
381 precipitation per Eq. (1). The FMI vulnerability map indicates that the Level 2 western Cordillera Ecoregion through  
382 northern Idaho (Fig. 1), a band of western Cordillera running north and south through west of central Washington and  
383 Oregon (which includes portions of the Cascade Range), and portions of the cold desert ecoregions in southeastern  
384 Washington and northwestern Arizona (Fig. 1) are more likely to see substantial changes to the FMI. The regional  
385 time series analyses (below) provide more information about whether those areas are expected to become wetter or  
386 drier. The seasonality vulnerability map identifies AUs that are likely to have changes in seasonality. Portions of the  
387 western Cordillera Ecoregion (Fig. 1; which includes the Sierra-Nevada Mountains in California, the Cascade  
388 Mountains in Washington and Oregon, and transitional terrain in Idaho) are projected to be more vulnerable to changes  
389 in seasonality. Otherwise, large portions of the study area are not projected to be vulnerable to changes for seasonality.

### 390 **3.2.1 Vulnerability of hydrologic landscapes**

391 Table 4 summarizes an analysis of the HL classifications of the most vulnerable AUs for each metric. For example,  
392 75 % of the AUs identified as vulnerable for snow accumulation (SWE) were classified as dry, moist, or wet, therefore  
393 very wet, semi-arid, and arid AUs are less likely to be vulnerable to changes in snow accumulation. Likewise, 76 %  
394 of AUs vulnerable to changes in seasonality had a spring seasonality during the 1971–2000 normal period. The  
395 physical properties represented by the dominant HL classes in Table 4 could help determine how various climate  
396 vulnerabilities are ultimately expressed. For example, vulnerability to changes in snow or FMI mostly occur in regions  
397 with wetter climates (Moist, Wet, or Very Wet climate), with fall or spring seasonality, in areas with low subsurface  
398 permeability. This could result in increased precipitation, with quicker runoff in areas that currently have delayed  
399 release of water. Similarly, areas vulnerable to changes in surface runoff are arid landscapes with winter seasonality

400 and highly permeable subsurface parent materials. This means that these changes in runoff could have a large impact  
401 on subsurface recharge and, ultimately, baseflow.

### 402 **3.2.2 Case studies & locational time series**

403 Hydrologic vulnerability analyses have been performed for a total of 45 exposure areas of ecological, economic, or  
404 social significance (Fig. 1 and Table 2; see Appendix A (Fig. A2)). The vulnerability index for each location is also  
405 listed in Table 2 for each metric. Three case study locations that are of economic interest are explored in detail and  
406 include Mt. Hood (Site #7), Willamette Valley (Site #9), Napa-Sonoma Valley (Site #28). During the normal period,  
407 61 % of the 1867 km<sup>2</sup> Napa-Sonoma Valley had an MwHMH HL classification, thus much of the area was classified  
408 as having a moist climate with winter seasonality, high subsurface permeability, mountain terrain, and high surface  
409 permeability. Eighty-three percent of the 1234 km<sup>2</sup> Willamette Valley AUs had an HL code of WfHHTH during the  
410 normal period. Overall, the Willamette Valley had a wet climate, dominated by fall seasonality, high subsurface  
411 permeability, transitional terrain, and high surface permeability. Table 2 indicates that 81 % of the 834 km<sup>2</sup> area  
412 analyzed for Mt. Hood had an HL code of VsHMH (very wet climate with spring seasonality, high subsurface  
413 permeability, mountainous terrain, and high surface permeability).

414 Figure 5 depicts line graphs of the historic and projected changes for the three case study locations (Mt. Hood (Site  
415 #7), Willamette Valley (Site #9), Napa-Sonoma Valley (Site #28)). The number in the lower left corner of each graph  
416 in Fig. 5 indicates the vulnerability index for the specific metric and location. For instance, precipitation at Mt. Hood  
417 has a vulnerability index of ‘3’, which indicates that three of the climate projections exceed the threshold of two-  
418 standard deviations from the historic mean.

419 The time series in Fig. 5 (and Fig. A2) illustrate the trend in average decadal temperature, precipitation, SWE, PET,  
420 climate, seasonality of water surplus and S’. Note that each future (2041–2070) climate projection is represented by a  
421 single data point that characterizes the 2041 – 2070 30-year range and is connected in Fig. 5 to the 2001–2010 decade  
422 with a dotted red line. Additional figures for 42 other locations are provided in Appendix A (Fig. A2). Given that Figs.  
423 5 and A2 represent case study examples, Figs. 4 and S6 provide better insight into the spatial distributions of the  
424 vulnerability assessments for the Western and continental U.S. Each of the three example case studies is predicted to  
425 be warmer in the 2041–2070 future climate projections. Further, these projected temperatures are almost always  
426 outside of the historic (1901–2010) temperature range, and so all locations have high vulnerability with respect to  
427 future temperatures. None of the three case studies show a strong trend relating to future precipitation projections. Mt.  
428 Hood appears to exhibit increasing precipitation since 1901, but there is no evidence that the projected increases in  
429 precipitation are outside of historic behavior, and so the site has low vulnerability for that metric. Napa-Sonoma and  
430 the Willamette Valley have low vulnerability for change in snow, while Mt. Hood has high vulnerability for April 1  
431 snow water equivalent in the 2041–2070 period. PET is calculated directly from temperature and so its vulnerability  
432 is strongly correlated to temperature. There are no obvious trends in S’ for the future projections in the three case  
433 studies; vulnerability of these sites for S’ is low to moderate. The FMI projections for Napa-Sonoma Valley, the  
434 Willamette Valley, and Mt. Hood are outside of two-standard deviations of historical trends in three to four out of ten

435 of the projections (Table 2). In terms of seasonality, the vulnerability index is equal to zero in the Willamette and  
436 Napa-Sonoma Valleys. For Mt. Hood, vulnerability is low, with all the future climate projections indicating that there  
437 will no longer be spring seasonality (the predominant historical season for runoff). Only three climate models suggest  
438 that decadal seasonality would transition to winter seasonality, which has not occurred since at least 1901.

## 439 **4 Discussion**

### 440 **4.1 Analyses of Retrospective and Projected Climate and Hydrologic Vulnerability**

441 Vulnerability maps (Fig. 4) were developed to facilitate long-term planning for stakeholders for assessing their risk to  
442 climatic impacts. It is possible that ecosystems, businesses, and communities in areas mapped as vulnerable may  
443 struggle to adapt to stresses imposed by future environmental conditions. As mentioned previously, the vulnerability  
444 index offers no information about the directions of change projected by the ten different models. Further, the RCP 8.5  
445 pathway was selected because it most closely resembles observed conditions (Schwalm et al., 2020).

446 The consistently projected high temperature vulnerability could lead to problems related to heat stress (e.g., human-  
447 related physical and mental health issues), urban heat islands (particularly in areas with little tree cover), and other  
448 temperature related problems (USGCRP, 2018). PET vulnerability would be problematic for agricultural systems,  
449 forest disease, and sectors that are drought sensitive (USGCRP, 2018). Precipitation vulnerability maps are important  
450 in specific areas with regards to flooding, landslides, and drought sensitivities. The vulnerability maps for snow  
451 accumulation and S' (surplus water available for runoff or infiltration) show that the areas mapped as most vulnerable  
452 for the two metrics are almost reversed, other than central Idaho and the coastal areas of California, Oregon, and  
453 Washington. According to the snow vulnerability map, it appears that most areas that receive large amounts of snow  
454 are projected to experience significant changes in future snow accumulation. In a related study on snow cover, Nolin  
455 and Daly (2006) found that the areas with the warmest winter temperatures are most at risk of having no snow cover  
456 in the future. Areas vulnerable for snow could impact not only the ski industry, but also water supply and streamflows,  
457 while the surplus water availability (S') vulnerability metric relates more directly to streamflow and flooding. Most  
458 of the study area is not vulnerable to changes in FMI (Fig. 4), which is an assessment of overall water availability,  
459 although some areas are more vulnerable (the Willamette Valley in Oregon, east of Puget Sound in Washington, and  
460 the northern panhandle in Idaho). The vulnerability map for seasonality (Fig. 4) shows that portions of the Western  
461 Cordillera (Fig. 1) including the high Sierra-Nevada mountains in California, the Cascade mountains in Oregon and  
462 Washington, and the mountainous areas in Idaho), have higher vulnerability indices, which indicates susceptibility  
463 regarding water supply, flooding, and streamflows.

464 Our retrospective analysis of PRISM time series data provided an understanding of environmental conditions since  
465 1901. We are aware of a few that have used retrospective analyses to inform their mapping efforts (Deviney et al.,  
466 2006; Kim et al., 2011; O'Brien et al., 2004), but are not aware of studies that have mapped resource vulnerability at  
467 a large scale using such data. Our definition of vulnerability is based on agreement of climate models leading to  
468 conditions that are outside of historic ranges. Our hypothesis is that systems experiencing future climate conditions  
469 outside of the historic range will not have the capacity to adapt to future conditions, and therefore are vulnerable. The

470 vulnerability issue is complicated by the fact that these vulnerability maps (Fig. 4) do not show how downstream areas  
471 could be impacted by these changes.

472 These vulnerability factors may be of interest to resource managers and decision makers, some of whom might  
473 consider high vulnerability for a single metric to be problematic. Yet for others, the additive or multiplicative impacts  
474 of numerous vulnerabilities may be of greater concern. For example, urban areas might be more impacted when  
475 vulnerable to multiple metrics, whereas PET vulnerability could be detrimental to agricultural or forested areas.  
476 Similarly, changes in seasonality from a snow dominated system to rain could have profound implications across  
477 many sectors.

478 For this analysis, the 30-year normal climate conditions were compared to decadal climate conditions since 1901. In  
479 addition, the 30-year normals for future projections (2041-2070) were compared to the historic range of decadal  
480 climate data. While comparing 30-year normals in a decadal analysis might appear to be a discrepancy in the analysis,  
481 the intention was to conservatively quantify vulnerability indices. 30-year normals exhibit less variability than decadal  
482 averages or annual averages. By comparing decadal averages to the 30-year future climate normals, we are not treating  
483 past data the same as future climate projections. However, the resulting vulnerability conclusions are conservative,  
484 because if we had used decadal projections for future climate data, variability in the range of output would have  
485 increased and our vulnerability indices could have increased for all parameters.

#### 486 **4.2 Hydrologic Response and Hydrologic Landscape Classification**

487 The HL Class for an AU can provide insight into its hydrological response, given changes in the quantity (FMI) or  
488 timing of surplus water (seasonality) on a landscape. Yet these factors only account for a portion of the water balance.  
489 However, when moisture is available as surface runoff, it may infiltrate into the ground or act as surface runoff,  
490 depending on the HL surface permeability class. Water may enter and flow through the subsurface layers (depending  
491 on the HL subsurface permeability) towards a stream channel. If the water was directed as surface or subsurface runoff,  
492 it may be transported more quickly in the downhill direction and into a stream channel depending upon the HL terrain  
493 class, which governs steepness. As it relates to streamflow, the unique combination of the five HL characteristics  
494 (climate, seasonality, surface permeability, subsurface permeability, and terrain) allows for the hydrologic response  
495 to be assessed relative to changes in temperature and climate (Leibowitz et al., 2014; Patil et al., 2014). At its most  
496 coarse application as it relates to this study, the transition from spring to winter seasonality for the Mt. Hood case  
497 study would result in a shorter ski season with snow conditions that could be less ideal for winter sports. However,  
498 this transition would also have many downstream impacts that could include flooding or habitat impacts. The HL  
499 approach could also be used to determine any relationships between HL characteristics and hydrologic vulnerability,  
500 while case studies can show how the HLVA could be useful.

#### 501 **4.3 Case studies**

502 Case studies are useful for illustrating how future climate conditions may impact important economic and conservation  
503 resources. It is necessary for a stakeholder to understand the parameters most important to their ecosystem, industry,  
504 or resource of interest, so that they can utilize location specific information about their potential climatic impacts  
505 (Glick et al., 2011; Lawler et al., 2010). In Fig. 5, case study examples (Mt. Hood (Site #7), Willamette Valley (Site  
506 #9), Napa-Sonoma Valley (Site #28)) demonstrate how the HLVA can assist in understanding how climate can impact  
507 important local water resources.

508 The wine and ski industries are important stakeholders in the western U.S. that may experience impacts from  
509 hydrological changes. The Napa-Sonoma and Willamette Valleys are known for their vineyards and associated  
510 wineries. Regarding their HL characteristics, they differ in their FMI class (Willamette is wet, whereas, Napa-Sonoma  
511 is moist) and their seasonality (Willamette has a fall seasonality, while Napa-Sonoma has a winter seasonality). Due  
512 to the importance of the pinot noir varieties in the Willamette Valley (Olen and Skinkis, 2018) and their temperature  
513 sensitivity (Burakowski and Magnusson, 2012; Jones et al., 2010), local viticulturalists are likely more concerned with  
514 changes in temperature than FMI. The Napa-Sonoma region is recognized for a variety of grape cultivars (Elliott-Fisk,  
515 1993) that are less sensitive to temperature fluctuations (Jones et al., 2010). Both the Willamette Valley and Napa-  
516 Sonoma have temperature vulnerability indices of ten out of ten, and both have FMI vulnerability indices of three out  
517 of ten (Fig. 5). These indices suggest that both locations are projected to have future temperatures that are different  
518 than historic temperatures. However, the Willamette Valley pinot noir grapes are more sensitive to temperature than  
519 in the Napa and Sonoma Valleys. In addition, while both locations have the same FMI vulnerability indices, Fig. 5  
520 illustrates that FMI projections for Napa-Sonoma are much more variable than for the Willamette Valley. Thus, there  
521 is more uncertainty in the modeled water availability for Napa-Sonoma. These results suggest that a vintner growing  
522 warm temperature grapes in the Willamette Valley may have more confidence in their investments relative to a vintner  
523 in Napa-Sonoma, where there is more uncertainty regarding long-term water availability.

524 The skiing industry is economically important, and the impact between a high and low snowfall year for the State of  
525 Oregon is \$38.1 million, while California is estimated to lose more than \$75 million in low snow years (Burakowski  
526 and Magnusson, 2012). Mt. Hood is known for its winter snow sports and tourism and would be impacted differently  
527 by the seven metrics than the Willamette and Napa-Sonoma case studies (Fig. 5). Thus, resource managers and  
528 business leaders at Mt. Hood are likely more concerned about snow accumulation in their watershed than those in the  
529 wine and grape industries (although grape grower's ability to irrigate may be impacted by snow accumulation in the  
530 region). According to our analyses, Mt. Hood is generally characterized by having a spring seasonality and has a snow  
531 vulnerability index of seven out of a maximum of ten. Also, the analysis of HL seasonality suggests some chance of  
532 a shorter ski season due to the risk of spring runoff occurring earlier and imposing on the winter season. Even though  
533 these conditions have occurred in the past (Fig. 5), this may be much more deleterious to the economics of the future  
534 ski industry than it was in the 1900s, because it contributed much less to the historic economy (for additional examples  
535 refer to Appendix A2).



536 **5 Summary and conclusions**

537 The hydrologic landscapes (HL) concept is useful for gaining a better understanding of hydrologic behavior at the  
538 assessment unit and watershed scales across large geographic regions. By applying the HL concept to climatic and  
539 vulnerability analyses, we provide a planning approach that allows resource managers to determine how vulnerable  
540 their location is to changes associated with climate that are important for a particular industry or application.  
541 Assessment of expected hydrologic response based upon physical and climatic characteristics has the potential to offer  
542 further insight into the idiosyncrasies of the threats faced by a stakeholder or industry across large geographic areas.  
543 This will allow them to make informed decisions about the risk imposed by potential changes that could affect their  
544 long-term planning efforts. The methodology also allows stakeholders to focus on specific areas of interest, which  
545 provides the flexibility necessary for the information to be relevant across applications and sectors. Examples of other  
546 phenomenon that could be examined using a similar or modified approach could include vulnerability associated with  
547 wildfire, landslides, and snowmelt related flooding, wetland persistence, flow permanence, among others. Other  
548 industries that could also be analyzed could include those associated with water reliant industries, such as agriculture  
549 (timber, fruit crops, seed crops, etc.), freshwater fisheries, and winter-tourism industries. By applying the modified  
550 Wigington et al. (2013) approach across the western U.S., resource managers will be able to base management  
551 decisions on assessments of climatic impacts of water resource-related vulnerabilities.

552 **6 Data availability**

553 The geospatial data files (Jones et al., 2020) will be uploaded to the GeoPlatform (<https://www.geoplatform.gov>) and  
554 EPA Environmental Dataset Gateway (<https://edg.epa.gov>). Data cannot be made publicly available and the DOI link  
555 cannot be activated until the paper is published per internal U.S. EPA policy.

556 **7 Code availability**

557 Authors may deposit code in a FAIR-aligned repository/archive upon final acceptance of the manuscript for  
558 publication.

559 **8 Video abstract**

560 No video abstract is available at this time.

561 **9 Author contribution**

562 CJ and SL conceptualized the study with significant input from KS. CJ performed the formal analyses, investigation,  
563 developed the methodologies (with input from SL, KS, and RC), managed the project, developed the model code,  
564 performed the analyses, developed the final figures and tables, and wrote draft versions of the manuscript, and  
565 incorporated co-author feedback into the final version of the manuscript. SL supervised the project and performed

566 project administration. RC contributed technical expertise regarding spatial data analyses and familiarity with  
567 hydrologic landscapes data analyses. RC and LS developed the subsurface permeability datasets. PM and CW  
568 provided the data and advice regarding the use of the future climate projections and the processing of those datasets.

## 569 **10 Acknowledgments**

570 We would like to thank James Markwiese, Mohammad Safeeq, Eric Sproles, and the three journal reviewers (including  
571 Shervan Gharari, Jason Todd, and one anonymous reviewer) for their constructive feedback on the manuscript. We  
572 also appreciate Jim Wigington's insight and input on early drafts of our mapping products. We acknowledge the World  
573 Climate Research Programme's Working Group on Coupled Modelling, which is responsible for CMIP, and we thank  
574 the climate modeling groups (listed in Table 1 of this paper) for producing and making available their model output.  
575 For CMIP the U.S. Department of Energy's Program for Climate Model Diagnosis and Intercomparison provides  
576 coordinating support and led development of software infrastructure in partnership with the Global Organization for  
577 Earth System Science Portals. The information in this document has been funded entirely by the U.S. Environmental  
578 Protection Agency, in part through an appointment to the Internship/Research Participation Program at the Office of  
579 Research and Development, U.S. Environmental Protection Agency, administered by the Oak Ridge Institute for  
580 Science and Education through an interagency agreement between the U.S. Department of Energy and EPA, and also  
581 through Student Services Contract #EP-15-W-000041. The views expressed in this paper are those of the authors and  
582 do not necessarily reflect the views or policies of the U.S. Environmental Protection Agency. Any use of trade, firm,  
583 or product names is for descriptive purposes only and does not imply endorsement by the U.S. Government.

## 584 **11 References**

- 585 Adger, W. N.: Vulnerability, *Glob. Environ. Chang.*, 16(3), 268–281, doi:10.1016/j.gloenvcha.2006.02.006, 2006.
- 586 Barnett, T. P., Adam, J. C. and Lettenmaier, D. P.: Potential impacts of a warming climate on water availability in  
587 snow-dominated regions, *Nature*, 438(7066), 303–309, doi:10.1038/nature04141, 2005.
- 588 Battin, J., Wiley, M. W., Ruckelshaus, M. H., Palmer, R. N., Korb, E., Bartz, K. K. and Imaki, H.: Projected impacts  
589 of climate change on salmon habitat restoration, *Proc. Natl. Acad. Sci. U. S. A.*, 104(16), 6720–6725,  
590 doi:10.1073/pnas.0701685104, 2007.
- 591 Brekke, L. D., Kiang, J. E., Olsen, J. R., Pulwarty, R. S., Raff, D. A., Turnipseed, D. P., Webb, R. S. and White, K.  
592 D.: Climate change and water resources management - A federal perspective: U.S. Geological Survey Circular 1331.,  
593 2009.
- 594 Burakowski, E. and Magnusson, M.: Climate impacts on the winter tourism economy in the United States, *Natl.*  
595 *Resour. Def. Counc.*, (December), 2012.
- 596 Bureau of Reclamation: Downscaled CMIP3 and CMIP5 Climate and Hydrology Projections: Release of Hydrology  
597 Projections, Comparison with preceding Information, and Summary of User Needs, Denver, Colorado, U.S.A., 2014.

598 Comeleo, R. L., Wigington Jr., P. J. and Leibowitz, S. G.: Creation of a digital aquifer permeability map for the Pacific  
599 Northwest (EPA/600/R-14/431), Corvallis, OR, USA., 2014.

600 Cook, B. I., Ault, T. R. and Smerdon, J. E.: Unprecedented 21st century drought risk in the American Southwest and  
601 Central Plains, *Sci. Adv.*, 1(1), e1400082, doi:10.1126/sciadv.1400082, 2015.

602 Daly, C.: A new effort to update precipitation frequency maps for the United States., 2016a.

603 Daly, C.: PRISM Climate Group, Oregon State University, [online] Available from: <http://prism.oregonstate.edu>,  
604 2016b.

605 Daly, C., Taylor, G. H., Gibson, W. P., Parzybok, T. W., Johnson, G. L. and Pasteris, P. A.: High-quality spatial  
606 climate data sets for the United States and beyond, *Trans. ASAE*, 43(6), 1957–1962, doi:10.13031/2013.3101, 2000.

607 Dettinger, M., Redmond, K. and Cayan, D.: Winter orographic precipitation ratios in the Sierra Nevada—Large-scale  
608 atmospheric circulations and hydrologic consequences, *J. Hydrometeorol.*, 5(6), 1102–1116, doi:10.1175/JHM-390.1,  
609 2004.

610 Dettinger, M. D.: Climate change, atmospheric rivers, and floods in California - A multimodel analysis of storm  
611 frequency and fagnitude changes, *J. Am. Water Resour. Assoc.*, 47(3), 514–523, doi:10.1111/j.1752-  
612 1688.2011.00546.x, 2011.

613 Deviney, F. A., Rice, K. C. and Hornberger, G. M.: Time series and recurrence interval models to predict the  
614 vulnerability of streams to episodic acidification in Shenandoah National Park, Virginia, *Water Resour. Res.*, 42(9),  
615 doi:10.1029/2005WR004740, 2006.

616 Dhungel, S., Tarboton, D. G., Jin, J. and Hawkins, C. P.: Potential Effects of Climate Change on Ecologically Relevant  
617 Streamflow Regimes, *River Res. Appl.*, 32(9), 1827–1840, doi:10.1002/rra.3029, 2016.

618 Elliott-Fisk, D. L.: Viticultural soils of California, with special reference to the Napa Valley, *J. Wine Res.*, 4(2), 67–  
619 74, 1993.

620 ESRI: ArcGIS Desktop, [online] Available from: <http://www.esri.com/>, 2016.

621 Farley, K. A., Tague, C. and Grant, G. E.: Vulnerability of water supply from the Oregon Cascades to changing  
622 climate: Linking science to users and policy, *Glob. Environ. Chang.*, 21(1), 110–122,  
623 doi:10.1016/j.gloenvcha.2010.09.011, 2011.

624 Feddema, J. J.: A revised Thornthwaite-type global climate classification, *Phys. Geogr.*, 26(6), 442–466,  
625 doi:10.2747/0272-3646.26.6.442, 2005.

626 Füssel, H. M.: Vulnerability: A generally applicable conceptual framework for climate change research, *Glob.*  
627 *Environ. Chang.*, 17(2), 155–167, doi:10.1016/j.gloenvcha.2006.05.002, 2007.

628 Füssel, H. M. and Klein, R. J. T.: Climate change vulnerability assessments: An evolution of conceptual thinking,  
629 *Clim. Change*, 75(3), 301–329, doi:10.1007/s10584-006-0329-3, 2006.

630 Glick, P., Stein, B. A. and Edelson, N. A., Eds.: Scanning the conservation horizon: A guide to climate change  
631 vulnerability assessment, National Wildlife Federation, Washington D.C., USA., 2011.

632 Hamlet, A. F.: Assessing water resources adaptive capacity to climate change impacts in the Pacific Northwest Region  
633 of North America, *Hydrol. Earth Syst. Sci.*, 15(5), 1427–1443, doi:10.5194/hess-15-1427-2011, 2011.

634 Hamon, W. R.: Estimating potential evapotranspiration, *J. Hydraul. Div.*, 87(3), 1961.

635 Hidalgo, H. G., Das, T., Dettinger, M. D., Cayan, D. R., Pierce, D. W., Barnett, T. P., Bala, G., Mirin, A., Wood, A.  
636 W., Bonfils, C., Santer, B. D. and Nozawa, T.: Detection and attribution of streamflow timing changes to climate  
637 change in the western United States, *J. Clim.*, 22(13), 3838–3855, doi:10.1175/2009JCLI2470.1, 2009.

638 Hijmans, R. J., Cameron, S. E., Parra, J. L., Jones, P. G. and Jarvis, A.: Very high resolution interpolated climate  
639 surfaces for global land areas, *Int. J. Climatol.*, 25(15), 1965–1978, doi:10.1002/joc.1276, 2005.

640 Hill, R. A., Hawkins, C. P. and Carlisle, D. M.: Predicting thermal reference conditions for USA streams and rivers,  
641 *Freshw. Sci.*, 32(1), 39–55, doi:10.1899/12-009.1, 2013.

642 Hill, R. A., Hawkins, C. P. and Jin, J.: Predicting thermal vulnerability of stream and river ecosystems to climate  
643 change, *Clim. Change*, 125(3–4), 399–412, doi:10.1007/s10584-014-1174-4, 2014.

644 IPCC: Climate Change 2014: Impacts, Adaptation, and Vulnerability, edited by C. B. Field, V. R. Barros, D. J.  
645 Dokken, K. J. Mach, M. D. Mastrandrea, T. E. Bilir, M. Chatterjee, K. L. Ebi, Y. O. Estrada, R. C. Genova, B. Girma,  
646 E. S. Kissel, A. N. Levy, S. MacCracken, P. R. Mastrandrea, and L. L. White, Cambridge University Press, Cambridge,  
647 UK and New York, NY, USA., 2014.

648 Jones, G. V., Duff, Andrew, A., Hall, A. and Myers, J. W.: Spatial analysis of climate in winegrape growing regions  
649 in the western United States, *Am. J. Enol. Vitic.*, 61, 313–326, 2010.

650 Jung, I. W. and Chang, H.: Climate change impacts on spatial patterns in drought risk in the Willamette River Basin,  
651 Oregon, USA, *Theor. Appl. Climatol.*, 108(3–4), 355–371, doi:10.1007/s00704-011-0531-8, 2012.

652 Kim, D. H., Yoo, C. and Kim, T. W.: Application of spatial EOF and multivariate time series model for evaluating  
653 agricultural drought vulnerability in Korea, *Adv. Water Resour.*, 34(3), 340–350,

654 doi:10.1016/j.advwatres.2010.12.010, 2011.

655 Lawler, J. J., Tear, T. H., Pyke, C., Shaw, R. M., Gonzalez, P., Kareiva, P., Hansen, L., Hannah, L., Klausmeyer, K.,  
656 Aldous, A., Bienz, C. and Pearsall, S.: Resource management in a changing and uncertain climate, *Front. Ecol.*  
657 *Environ.*, 8(1), 35–43, doi:10.1890/070146, 2010.

658 Leibowitz, S. G., Wigington Jr., P. J., Comeleo, R. L. and Ebersole, J. L.: A temperature-precipitation-based model  
659 of thirty-year mean snowpack accumulation and melt in Oregon, USA, *Hydrol. Process.*, 26, 741–759,  
660 doi:10.1002/hyp.8176, 2012.

661 Leibowitz, S. G., Comeleo, R. L., Wigington Jr., P. J., Weaver, C. P., Morefield, P. E., Sproles, E. A. and Ebersole, J.  
662 L.: Hydrologic landscape classification evaluates streamflow vulnerability to climate change in Oregon, USA, *Hydrol.*  
663 *Earth Syst. Sci.*, 18(9), 3367–3392, doi:10.5194/hess-18-3367-2014, 2014.

664 Leibowitz, S. G., Comeleo, R. L., Wigington Jr., P. J., Weber, M. H., Sproles, E. A. and Sawicz, K. A.: Hydrologic  
665 landscape characterization for the Pacific Northwest, USA, *J. Am. Water Resour. Assoc.*, 52(2), 473–493,  
666 doi:10.1111/1752-1688.12402, 2016.

667 Luce, C. H. and Holden, Z. A.: Declining annual streamflow distributions in the Pacific Northwest United States,  
668 1948–2006, *Geophys. Res. Lett.*, 36(16), 2–7, doi:10.1029/2009GL039407, 2009.

669 Mancosu, N., Snyder, R., Kyriakakis, G. and Spano, D.: Water Scarcity and Future Challenges for Food Production,  
670 *Water*, 7(3), 975–992, doi:10.3390/w7030975, 2015.

671 Mann, M. E. and Gleick, P. H.: Climate change and California drought in the 21st century:, *Proc. Natl. Acad. Sci.*,  
672 112(13), 3931–3936, doi:10.1073/pnas.1503667112, 2015.

673 Maurer, D. K., Lopes, T. J., Medina, R. L. and Smith, J. L.: Hydrogeology and hydrologic landscape regions of  
674 Nevada, Carson City, NV., 2004.

675 McAfee, S. A.: Methodological differences in projected potential evapotranspiration, *Clim. Change*, 120(4), 915–930,  
676 doi:10.1007/s10584-013-0864-7, 2013.

677 McKay, L., Bondelid, T., Dewald, T., Johnston, J., Moore, R. and Rea, A.: NHDPlus Version 2: User Guide., 2012.

678 Mekonnen, M. and Hoekstra, A.: Four Billion People Experience Water Scarcity, *Sci. Adv.*, (2), 1–7,  
679 doi:10.1126/sciadv.1500323, 2016.

680 Miller, D. A. and White, R. A.: A conterminous United States multi-layer soil characteristics data set for regional  
681 climate and hydrology modeling, *Earth Interact.* 2 [online] Available from: <http://earthinteractions.org>, 1998.

682 Mock, C. J.: Climatic controls and spatial variations of precipitation in the western United States, *J. Clim.*, 9(5), 1111–  
683 1124, doi:10.1175/1520-0442(1996)009<1111:CCASVO>2.0.CO;2, 1996.

684 Mote, P. W., Hamlet, A. F., Clark, M. P. and Lettenmaier, D. P.: Declining mountain snowpack in western North  
685 America, *Bull. Am. Meteorol. Soc.*, 86(1), 39–49, doi:10.1175/BAMS-86-1-39, 2005.

686 National Intelligence Council: Global Water Security: Intelligence Community Assessment (ICA 2012-08),  
687 Washington D.C., USA. [online] Available from: [https://www.dni.gov/files/documents/Special\\_Report\\_ICA\\_Global](https://www.dni.gov/files/documents/Special_Report_ICA_Global_Water_Security.pdf)  
688 [Water Security.pdf](https://www.dni.gov/files/documents/Special_Report_ICA_Global_Water_Security.pdf), 2012.

689 Nelson, G. C.: Chapter 3. Drivers of Ecosystem Change: Summary Chapter, Island Press, Washington D.C., USA.,  
690 2005.

691 Nijssen, B., O'Donnell, G. M., Hamlet, A. F. and Lettenmaier, D. P.: Hydrologic Sensitivity of Global Rivers to  
692 Climate Change, *Clim. Change*, 50(1), 143–175 [online] Available from:  
693 <http://www.springerlink.com/index/M24116121218031X.pdf> (Accessed 29 July 2011), 2001.

694 NOAA State Climate Extremes Committee: Climatic Extreme Records, NOAA Natl. Centers Environ. Inf. [online]  
695 Available from: <http://www.ncdc.noaa.gov/extremes/sceec/records> (Accessed 18 November 2018), 2016.

696 Nolin, A. W.: Perspectives on climate change, mountain hydrology, and water resources in the Oregon Cascades,  
697 USA, *Mt. Res. Dev.*, 32, S35–S46, doi:10.1659/MRD-JOURNAL-D-11-00038.S1, 2011.

698 Nolin, A. W. and Daly, C.: Mapping “at risk” snow in the Pacific Northwest, *J. Hydrometeorol.*, 7, 1164–1171,  
699 doi:10.1175/JHM543.1, 2006.

700 O'Brien, K., Leichenko, R., Kelkar, U., Venema, H., Aandahl, G., Tompkins, H., Javed, A., Bhadwal, S., Barg, S.,  
701 Nygaard, L. and West, J.: Mapping vulnerability to multiple stressors: Climate change and globalization in India,  
702 *Glob. Environ. Chang.*, 14(4), 303–313, doi:10.1016/j.gloenvcha.2004.01.001, 2004.

703 Olen, B. and Skinkis, P.: Vineyard Economics: Establishing and Producing Pinot Noir Wine Grapes in the Willamette  
704 Valley, Oregon, Oregon State Univ., (October), 1–19 [online] Available from:  
705 <https://agsci.oregonstate.edu/sites/agscid7/files/oaeb/pdf/aeb0060.pdf>, 2018.

706 Patil, S. D., Wigington Jr., P. J., Leibowitz, S. G. and Comeleo, R. L.: Use of hydrologic landscape classification to  
707 diagnose streamflow predictability in Oregon, *J. Am. Water Resour. Assoc.*, 50(3), 762–776, doi:10.1111/jawr.12143,  
708 2014.

709 Ramirez-Villegas, J. and Jarvis, A.: Downscaling global circulation model outputs: The delta method decision and  
710 policy analysis working paper No. 1, Cali, Columbia. [online] Available from: [22/57](http://ccafs-</a></p>
</div>
<div data-bbox=)

711 [climate.org/downloads/docs/Downscaling-WP-01.pdf](http://climate.org/downloads/docs/Downscaling-WP-01.pdf), 2010.

712 Safeeq, M., Grant, G. E., Lewis, S. L., Kramer, M. G. and Staab, B.: A hydrogeologic framework for characterizing  
713 summer streamflow sensitivity to climate warming in the Pacific Northwest, USA, *Hydrol. Earth Syst. Sci.*, 18(9),  
714 3693–3710, doi:10.5194/hess-18-3693-2014, 2014.

715 Schwalm, C. R., Glendon, S. and Duffy, P. B.: RCP8.5 tracks cumulative CO<sub>2</sub> emissions, *Proc. Natl. Acad. Sci.*,  
716 117(33), 19656–19657, doi:10.1073/pnas.2007117117, 2020.

717 Siler, N., Roe, G. and Durran, D.: On the dynamical causes of variability in the rain-shadow effect: A case study of  
718 the Washington Cascades, *J. Hydrometeorol.*, 14(1), 122–139, doi:10.1175/JHM-D-12-045.1, 2013.

719 Soil Survey Staff: Web Soil Survey, Nat. Resour. Conserv. Serv. USDA [online] Available from:  
720 <http://websoilsurvey.nrcs.usda.gov/> (Accessed 18 May 2016), 2016.

721 Stratton, L., Comeleo, R. L., Leibowitz, S. G. and Wigington Jr., P. J.: Development of a digital aquifer permeability  
722 map for the pacific southwest in support of the hydrologic landscape classification: Methods (EPA/600/R-16/063),  
723 Corvallis, OR, USA. [online] Available from:  
724 <https://nepis.epa.gov/Exe/ZyPDF.cgi/P100PB7N.PDF?Dockey=P100PB7N.pdf>, 2016.

725 Tague, C. and Grant, G. E.: A geological framework for interpreting the low-flow regimes of Cascade streams,  
726 Willamette River Basin, Oregon, *Water Resour. Res.*, 40(4), 1–9, doi:10.1029/2003WR002629, 2004.

727 Tague, C. L., Choate, J. S. and Grant, G.: Parameterizing sub-surface drainage with geology to improve modeling  
728 streamflow responses to climate in data limited environments, *Hydrol. Earth Syst. Sci.*, 17(1), 341–354,  
729 doi:10.5194/hess-17-341-2013, 2013.

730 Tansel, B.: Hydrologic vulnerability and preventing domino effect consequences, *Hydrol. Curr. Res.*, 4(4), 10–11,  
731 doi:10.4172/2157-7587.1000e11, 2013.

732 Taylor, K. E., Stouffer, R. J. and Meehl, G. A.: An overview of CMIP5 and the experiment design, *Bull. Am. Meteorol.*  
733 *Soc.*, 93(4), 485–498, doi:10.1175/BAMS-D-11-00094.1, 2012.

734 Thompson, D. W. and Wallace, J. M.: Regional climate impacts of the Northern Hemisphere annular mode, *Science*,  
735 293, 85–89, doi:10.1126/science.1058958, 2001.

736 Todd, M. J., Wigington Jr., P. J. and Sproles, E. A.: Hydrologic landscape classification to estimate Bristol Bay,  
737 Alaska watershed hydrology, *J. Am. Water Resour. Assoc.*, 53(5), 1008–1031, doi:[https://doi.org/10.1111/1752-](https://doi.org/10.1111/1752-1688.12544)  
738 1688.12544, 2017.

739 U.S. Environmental Protection Agency: A systematic approach for selecting climate projections to inform regional  
740 impact assessments (Final). EPA/600/R-20/309, 2020. [online] Available from:  
741 <https://cfpub.epa.gov/ncea/iclus/recordisplay.cfm?deid=349727>

742 U.S. Global Change Research Program: The United States National Climate Assessment. Uses of Vulnerability  
743 Assessments for the National Climate Assessment. NCA Report Series, Volume 9., Washington D.C., USA. [online]  
744 Available from: [http://www.globalchange.gov/browse/reports?f%5B0%5D=field\\_report\\_year:171](http://www.globalchange.gov/browse/reports?f%5B0%5D=field_report_year:171), 2011.

745 U.S. Global Change Research Program (USGCRP): Fourth National Climate Assessment, Washington D.C., USA.  
746 [online] Available from: <https://www.globalchange.gov>, 2018.

747 Vano, J. A., Nijssen, B. and Lettenmaier, D. P.: Seasonal hydrologic responses to climate change in the Pacific  
748 Northwest, *Water Resour. Res.*, 6(4), 1–18, doi:10.1002/2014WR015909, 2015.

749 Watson, J. E. M., Iwamura, T. and Butt, N.: Mapping vulnerability and conservation adaptation strategies under  
750 climate change, *Nat. Clim. Chang.*, 3(11), 989–994, doi:10.1038/nclimate2007, 2013.

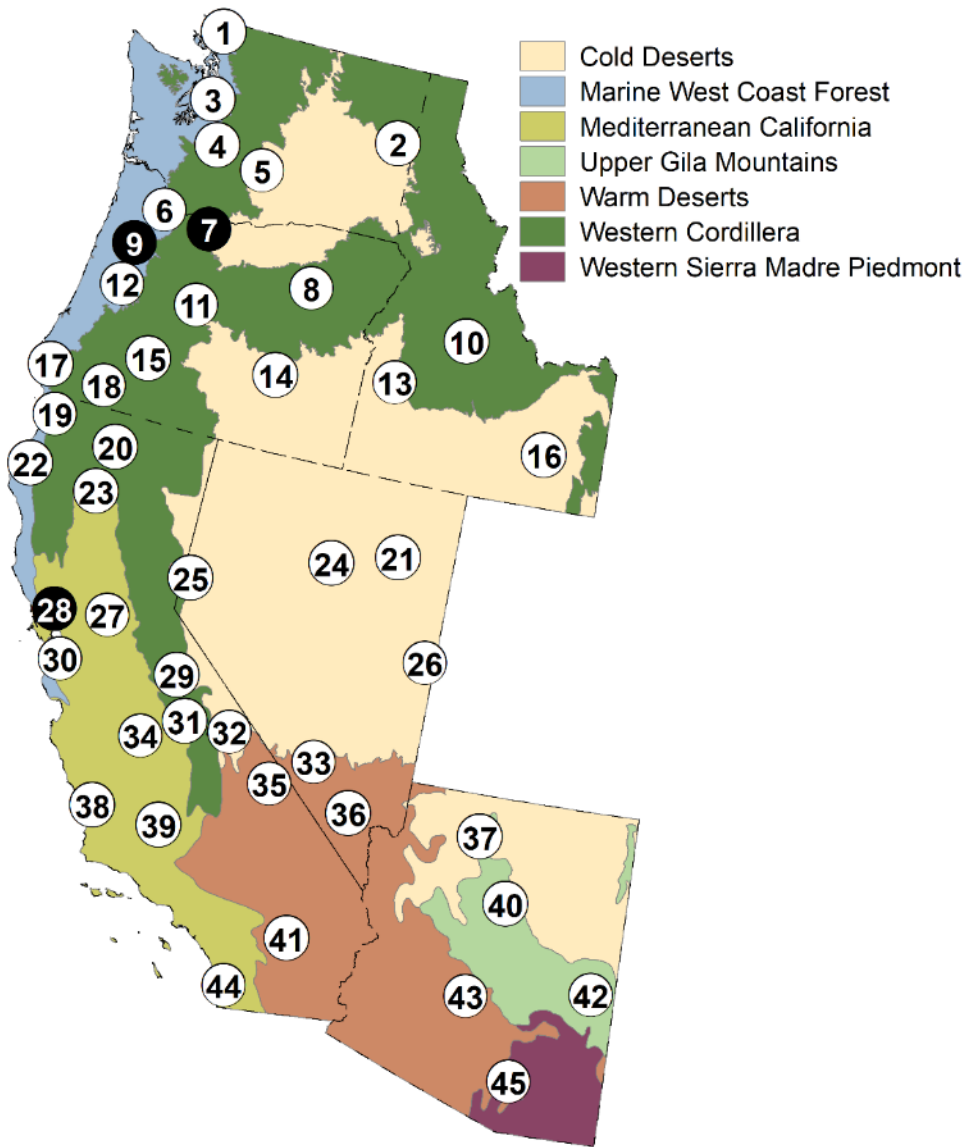
751 Wigington Jr., P. J., Leibowitz, S. G., Comeleo, R. L. and Ebersole, J. L.: Oregon hydrologic landscapes: A  
752 classification framework, *J. Am. Water Resour. Assoc.*, 49(1), 163–182, doi:10.1111/jawr.12009, 2013.

753 Winter, T. C.: The vulnerability of wetlands to climate change: a hydrologic landscape perspective, *J. Am. Water*  
754 *Resour. Assoc.*, 36(2), 305–311, doi:10.1111/j.1752-1688.2000.tb04269.x, 2000.

755 Winter, T. C.: The concept of hydrologic landscapes, *J. Am. Water Resour. Assoc.*, 37(2), 335–349, 2001.

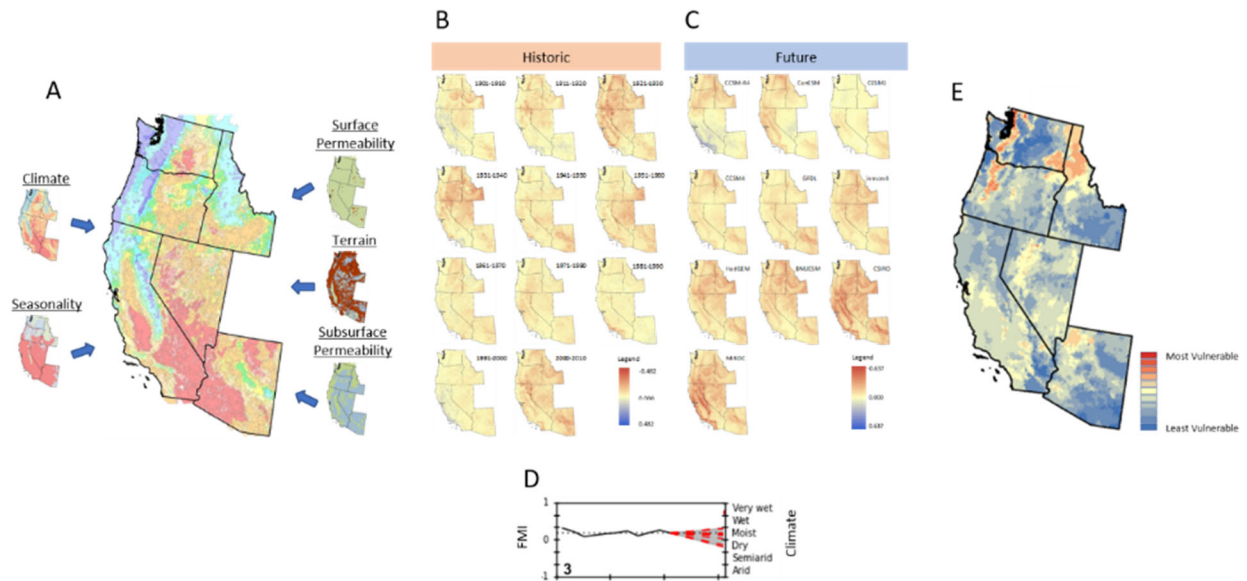
756 Wolock, D. M., Winter, T. C. and McMahon, G.: Delineation and evaluation of hydrologic-landscape regions in the  
757 United States using geographic information system tools and multivariate statistical analyses, *Environ. Manage.*, 34,  
758 S71–S88, doi:10.1007/s00267-003-5077-9, 2004.





760

761 Figure 1. Study area showing map with the six states of WA, OR, ID, CA, NV, and AZ. Also shown are the seven EPA Level  
762 II Ecoregions (<https://www.epa.gov/eco-research/ecoregions-north-america>) and 45 locations identified by numbered  
763 circles with three case study locations in black circles (Table 2). State boundaries are indicated by black dashed lines.

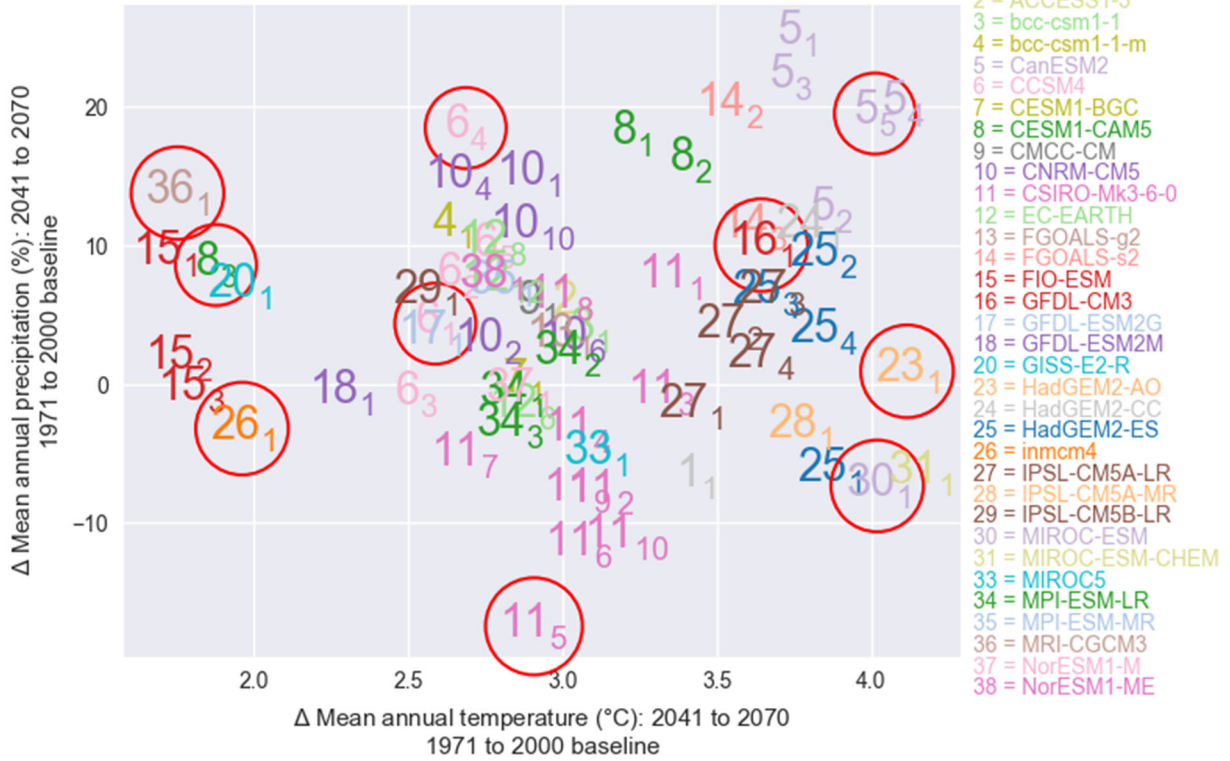


764

765 **Figure 2. Mapping of hydrologic vulnerability.** A) Hydrologic landscape map is developed for six western states using 1971-  
 766 2000 normals for climate (Feddema Moisture Index; FMI) and seasonality, along with surface permeability, terrain, and  
 767 subsurface permeability geophysical data. B) Historical decadal analysis is run from 1901 through 2010 for each of seven  
 768 metrics: monthly temperature, precipitation, potential evapotranspiration, surplus water, snow water equivalent, FMI  
 769 (shown), and seasonality. C) Future predicted behavior is estimated for each of the seven metrics, based on ten climate  
 770 model projections (FMI shown). D) Vulnerability is then defined as the number of climate projections that lie outside of the  
 771 historical two standard deviation threshold (example for FMI from Napa-Sonoma shown). E) Vulnerability values are then  
 772 mapped for each metric across the six-state study area (FMI shown).

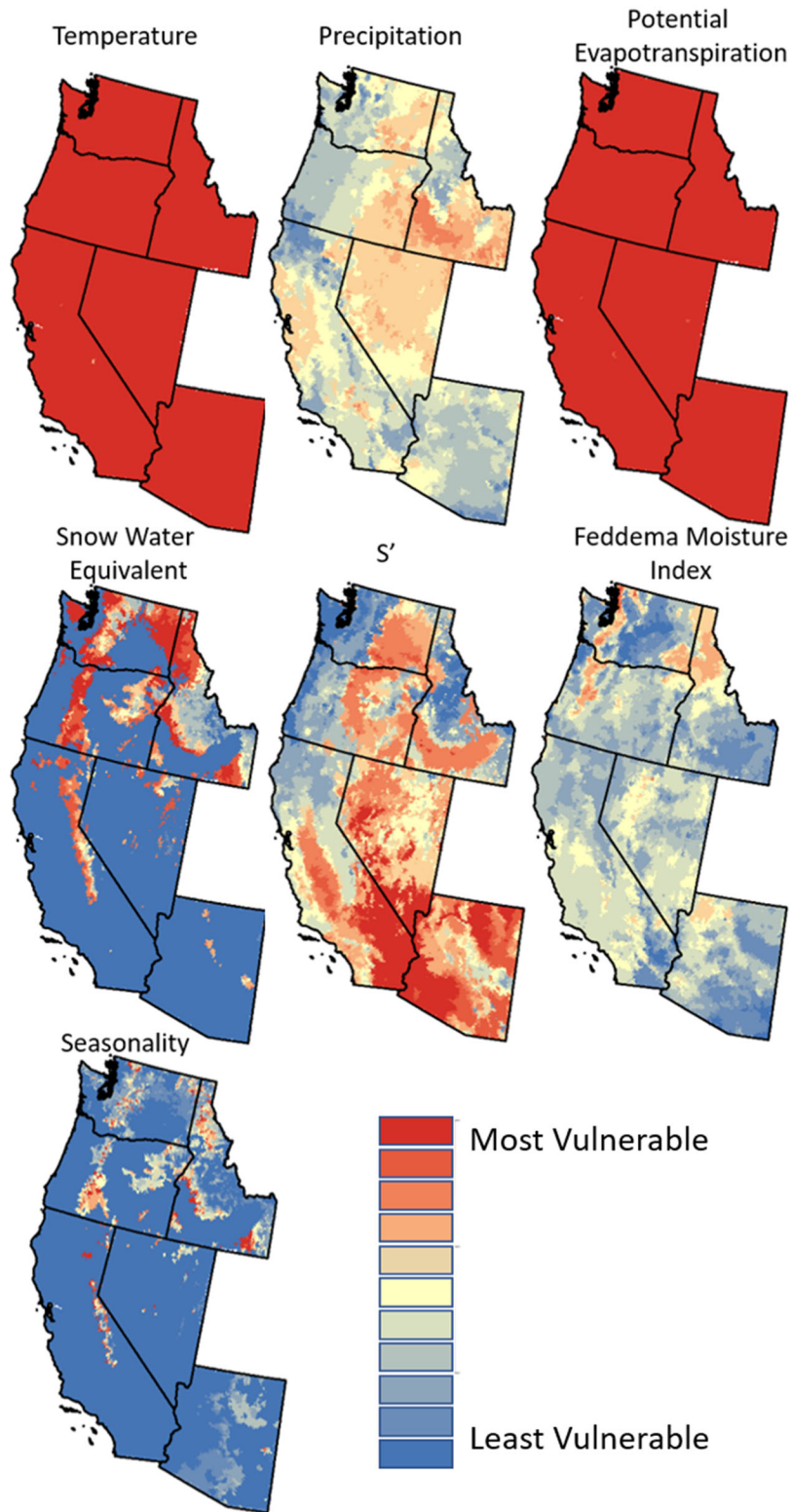
### 70 realizations of climate change from CMIP5 (BCSD)

Emissions Scenario: RCP85 Study area: AZ\_CA\_ID\_NV\_OR\_WA



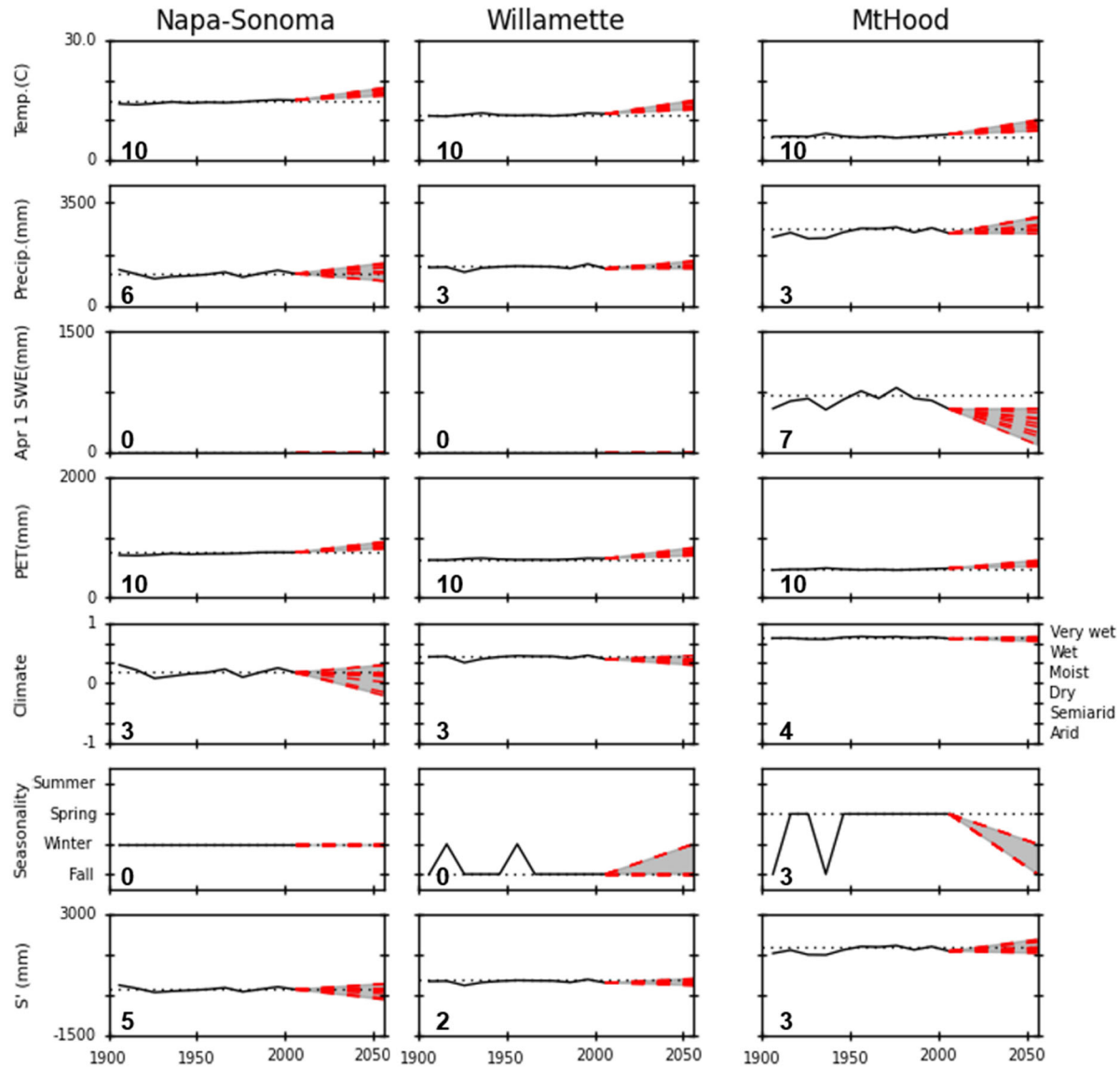
773  
 774 **Figure 3. Scatterplot showing the range of mean temperature and precipitation projections for the 2041–2070 climate**  
 775 **models across the study area. The circled data points identify the climate projections used in our analyses. Climate models**  
 776 **are enumerated using the key to the right of the scatterplot. Subscripts denote the realization number of each unique**  
 777 **projection. Legend colors are used to improve legibility where scatterplot symbols overlap.**

778



779

780 **Figure 4. Vulnerability indices for temperature, precipitation, potential evapotranspiration, snow water equivalent (April**  
 781 **1), S' (available water), Feddema Moisture Index, and seasonality. The least vulnerable locations are those projected to be**  
 782 **within two-standard deviations of the historic (1901–2010) mean in all ten climate models.**



783

784 Figure 5. Time series of average decadal temperature, precipitation, snow (April 1 snow water equivalent (mm)), potential  
 785 evapotranspiration (PET), climate (FMI), seasonality, and available water (S') for three specific locations in the western  
 786 U.S. For the climate / FMI figures, the FMI values range from 1 to -1 (primary y-axis on the left), whereas the categorical  
 787 version of the index ranges from arid to very wet (secondary y-axis on the right). Dotted black line represents the 1971–  
 788 2000 base period; the dashed red line connects the 2001–2010 value to the 2041–2070 climate projections for each of the  
 789 ten models. The gray shaded area represents the range of model projections. The number in lower left indicates the  
 790 vulnerability index for the metric and location depicted in the associated graph.

791 **13 Tables**

792 **Table 1. CMIP5 Climate model summary for 2041–2070 precipitation and temperature data** (Bureau of Reclamation, 2014).

<b>WCRP CMIP5 Climate Model</b>	<b>Model abbreviated name</b>	<b>Model realization used herein</b>	<b>Abbreviated name used in Figure 3 for realization</b>
Canadian Earth System Model	CanESM2	r5i1p1	CanESM2
Community Climate System Model	CCSM4	r1i1p1	CCSM4
Community Climate System Model	CCSM4	r4i1p1	CCSM4-R4
Community Earth System Model	CESM1	r3i1p1	CESM1
Commonwealth Scientific and Industrial Research Organisation Mark 3.6	CSIRO-Mk3-6-0	r5i1p1	CSIRO
Geophysical Fluid Dynamics Laboratory Coupled Climate Model	GFDL-CM3	r1i1p1	GFDL
Hadley Global Environment Model	HadGEM2-AO	r1i1p1	HadGem
Institute for Numerical Mathematics Climate Model	INM-CM4	r1i1p1	inmcm4
Model for Interdisciplinary Research on Climate	MIROC-ESM	r1i1p1	MIROC
Meteorological Research Institute	MRI-CGCM3	r1i1p1	MRI-CGCM3

793

794 **Table 2. Summary table for 45 study locations (sorted by decreasing latitude) providing numeric ID from Fig. 1, total analysis area, dominant HL class (representing**  
795 **climate, seasonality, subsurface permeability, terrain, and surface permeability), percent area represented by dominant HL class, latitude and longitude of the center point**  
796 **of the area, and vulnerability indices for temperature, precipitation, potential evapotranspiration (PET), surplus water (S'), snow water equivalent (snow), Feddema**  
797 **Moisture Index (FMI), and seasonality.**

Site #	Name	Area (km <sup>2</sup> )	Dominant HL Class*	% Dominant Area	Coordinates		Vulnerability Index						
					Lat.	Long.	Temp.	Pre cip.	PET	S'	Snow	FMI	Seasonality
1	Bellingham	212	WfLTH	99 %	48.77	-122.45	10	5	10	1	0	9	0
2	Spokane	592	DfHHTH	80 %	47.64	-117.43	10	6	10	7	10	3	1
3	Seattle	669	WfLTH	78 %	47.60	-122.25	10	4	10	1	0	5	2
4	Mt Rainier	718	VsLMH	76 %	46.85	-121.79	10	4	10	2	7	4	2
5	Yakima	438	SfHHTH	86 %	46.63	-120.60	10	3	10	6	0	0	0
6	Portland	932	WfHHTH	67 %	45.53	-122.66	10	3	10	2	0	6	0
7	Mt. Hood	834	VsHMH	81 %	45.37	-121.70	10	3	10	3	7	4	3
8	Umatilla NF	2,147	MsLMH	29 %	44.87	-118.70	10	6	10	3	6	3	4
9	Willamette	1,234	WfHHTH	83 %	44.84	-123.14	10	3	10	2	0	4	0
10	Challis NF	4,348	WsLMH	74 %	44.55	-114.75	10	6	10	0	3	2	0
11	Bend	948	SfHHTH	68 %	44.21	-121.26	10	4	10	8	0	3	0
12	Eugene	523	WfHFH	64 %	44.10	-123.15	10	3	10	1	0	2	0
13	Boise	594	SwHHTH	51 %	43.61	-116.24	10	8	10	8	0	2	0
14	Malheur NWR	1,355	SwHFH	69 %	43.27	-119.04	10	6	10	7	0	2	0
15	Crater Lake	1,721	WsHHTH	45 %	42.98	-122.08	10	3	10	2	9	3	10

Site #	Name	Area (km <sup>2</sup> )	Dominant HL Class*	% Dominant Area	Coordinates			Vulnerability Index					
					Lat.	Long.	Temp.	Pre cip.	PET	S'	Snow	FMI	Seasonality
16	Pocatello	349	DwHTH	45 %	42.88	-112.43	10	7	10	7	0	1	0
17	Siskiyou NF	926	VwLMH	100 %	42.36	-124.29	10	2	10	0	0	2	0
18	Medford	375	DfLTH	60 %	42.34	-122.89	10	1	10	5	0	2	0
19	Six Rivers	1,527	VwLMH	100 %	41.63	-123.79	10	2	10	2	0	4	0
20	Mt Shasta	956	WwHMH	49 %	41.36	-122.23	10	1	10	2	0	3	0
21	Ruby Mtn	1,132	DfLTH	44 %	40.68	-115.31	10	6	10	5	9	4	0
22	Arcata-Humboldt Co	2,511	WwLMH	63 %	40.62	-124.01	10	3	10	2	0	3	0
23	Redding	478	MwHTH	59 %	40.56	-122.38	10	2	10	2	0	2	0
24	Battle Mtn	902	SwLMH	75 %	40.09	-116.71	10	6	10	7	0	4	0
25	Reno	382	SwHTH	40 %	39.54	-119.80	10	4	10	7	0	3	0
26	Great Basin NP	38	MsLMH	100 %	39.01	-114.26	10	4	10	5	0	4	1
27	Sacramento	855	SwHFH	88 %	38.57	-121.39	10	6	10	7	0	3	0
28	Napa-Sonoma	1,867	MwHTH	61 %	38.37	-122.53	10	6	10	5	0	3	0
29	Yosemite NP	2,455	VsLMH	44 %	37.93	-119.55	10	4	10	4	9	3	0
30	San Francisco Bay	3,356	DwHMH	19 %	37.44	-122.29	10	6	10	5	0	5	0
31	Sierra NF	5,349	WwLMH	31 %	37.17	-119.05	10	4	10	4	0	2	0
32	High Sierras	2,239	WsLMH	32 %	37.15	-118.81	10	2	10	4	1	2	0



Site #	Name	Area (km <sup>2</sup> )	Dominant HL Class*	% Dominant Area	Coordinates		Temp.	Pre cip.	Vulnerability Index				
					Lat.	Long.			PET	S'	Snow	FMI	Seasonality
33	Nevada Test Site	3,121	AwHMH	67 %	36.96	-116.22	10	5	10	10	0	4	0
34	Fresno	1,393	AwHFH	100 %	36.74	-119.91	10	5	10	8	0	4	0
35	Death Valley NP	7,862	AwHMH	50 %	36.45	-117.03	10	5	10	10	0	5	0
36	Las Vegas	977	AwHTH	65 %	36.23	-115.26	10	4	10	10	0	4	0
37	Grand Canyon NP	3,475	SwHMH	28 %	36.22	-112.11	10	4	10	10	0	6	0
38	San Luis Obispo	2,653	DwLMH	98 %	35.36	-120.63	10	4	10	4	0	4	0
39	Bakersfield	3,399	AwHFH	96 %	35.33	-119.14	10	4	10	9	0	4	0
40	Flagstaff	365	DwHMH	51 %	35.19	-111.60	10	3	10	4	0	4	0
41	Joshua Tree NP	2,599	AwLMH	68 %	33.92	-115.99	10	5	10	7	0	5	0
42	White Mtns	4,855	WfLMH	23 %	33.87	-109.53	10	4	10	3	0	3	0
43	Phoenix	2,304	AwHFH	63 %	33.52	-112.11	10	3	10	10	0	2	1
44	San Diego	1,276	SwLMH	37 %	32.90	-117.06	10	4	10	6	0	4	0
45	Tucson	1,838	AwHTH	62 %	32.19	-110.95	10	3	10	9	0	1	2

798 \*Climate class (1st letter): V=very wet; W=wet; M=moist; D=dry; S=semiarid; A=arid

799 Seasonality class (2nd letter): f=fall; w= winter; s=spring; u=summer

800 Subsurface permeability class (3rd letter): L=low; H=high

801 Terrain class (4th letter): M=mountain; T=transitional; F=flat

802 Surface permeability class (5th letter): L=low; H=high

803 **Table 3. Percent of area of each HL category and classification within the six-state region (1971–2000)**

Category	Classification	Area (%)
Climate	Arid	21 %
	Semi-arid	34 %
	Dry	15 %
	Moist	9 %
	Wet	14 %
	Very wet	7 %
Season	Spring (AMJ <sup>1</sup> )	13 %
	Summer (JAS <sup>2</sup> )	1 %
	Fall (OND <sup>3</sup> )	24 %
	Winter (JFM <sup>4</sup> )	63 %
Subsurface Permeability	Low	40 %
	High	60 %
Terrain	Flat	7 %
	Transitional	63 %
	Mountain	30 %
Surface Permeability	Low	2 %
	High	98 %

804 <sup>1</sup>AMJ: April, May, and June

805 <sup>2</sup>JAS: July, August, and September

806 <sup>3</sup>OND: October, November, and December

807 <sup>4</sup>JFM: January, February, and March

808 **Table 4. Hydrologic landscape characteristics of assessment units identified as vulnerable (having a vulnerability index**  
 809 **greater than 7 on a scale of 10) for each metric.**

		% Assessment units that share HL classification									
		Climate <sup>1</sup>		Seasonality <sup>2</sup>		Subsurface Permeability <sup>3</sup>		Terrain <sup>4</sup>		Surface permeability <sup>3</sup>	
Vulnerability Parameter	Temperature	70 %	D, S, or A	87 %	f or w	60 %	H	93 %	M or T	98 %	H
	Precipitation	72 %	D or S	79 %	f or w	71 %	H	97 %	M or T	98 %	H
	PET	70 %	D, S, or A	87 %	f or w	60 %	H	93 %	M or T	98 %	H
	Surplus water (S <sup>+</sup> )	92 %	A or S	79 %	w	75 %	H	87 %	M or T	99 %	H
	Snow water equivalent (SWE)	75 %	D, M, or W	87 %	f or s	53 %	L	82 %	M	100 %	H
	FMI	71 %	V or W	65 %	f	75 %	L	75 %	M	100 %	H
	Seasonality	75 %	W or M	76 %	s	51 %	H	83 %	M	99 %	H

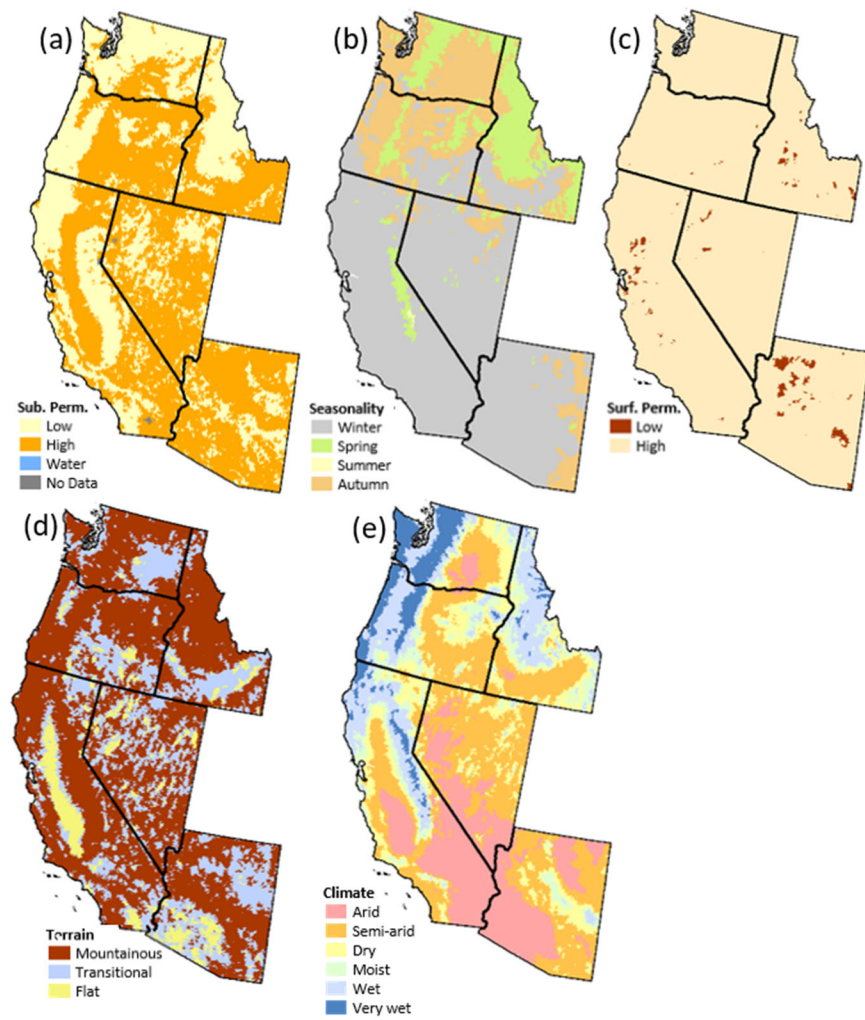
810 <sup>1</sup>A=arid, S=semiarid, D=dry, M=moist, W=wet

811 <sup>2</sup>f=fall, w=winter, s=spring

812 <sup>3</sup>L=low, H=high

813 <sup>4</sup>T=transitional, M=mountainous

814

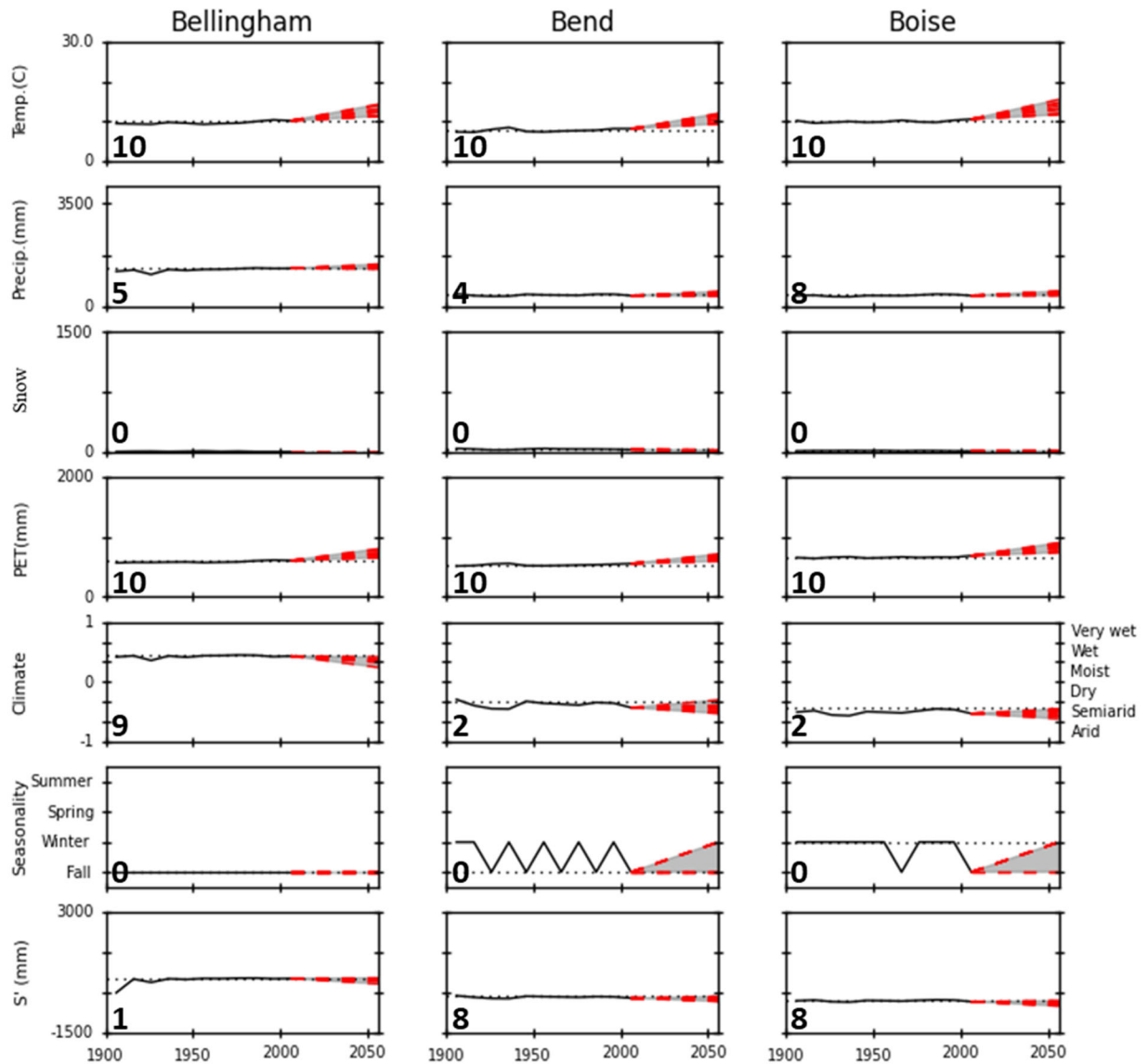


816

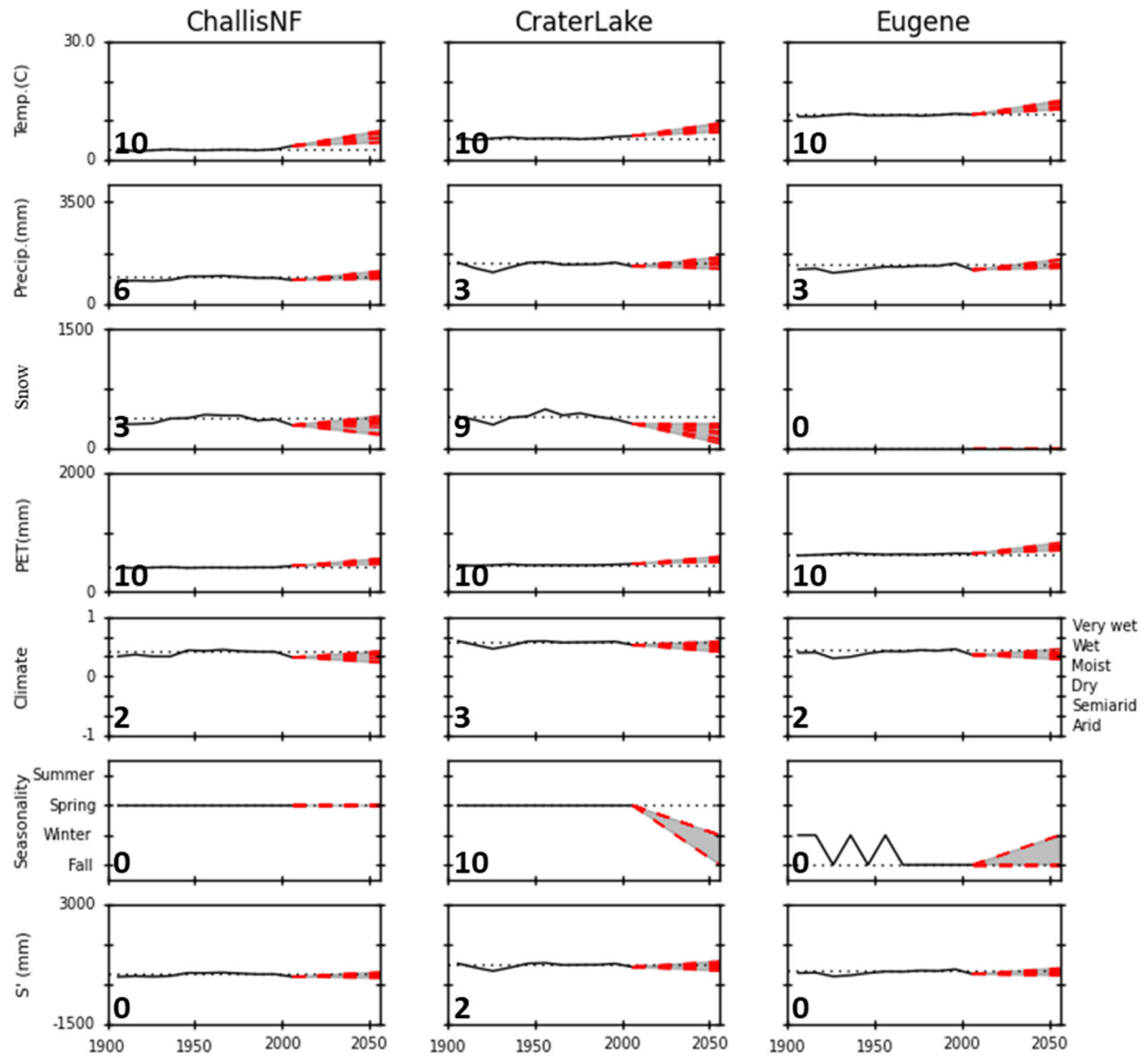
817 **Figure A1. Component Hydrologic Landscape maps of Washington, Idaho, Oregon, California, Nevada, and Arizona were**  
 818 **used in the analysis of the HLVA indices [(a) Subsurface Permeability, (b) Seasonality of precipitation surplus, (c). Surface**  
 819 **permeability, (d) Climate, and (e) Terrain]. Notes: The seasonality map for the PNW has been updated from the original**  
 820 **Leibowitz et al. 2016 HL map, as we separated their winter seasonality into two seasons (winter and fall).**

821 **Figure A2**

822 **Time series of average decadal temperature, precipitation, snow (April 1 snow water equivalent), potential**  
 823 **evapotranspiration (PET), climate (FMI), seasonality, and available water (S') for 45 specific locations in the western U.S.**  
 824 **For the climate / FMI figures, the FMI values range from 1 to -1 (primary y-axis on the left), whereas the categorical version**  
 825 **of the index ranges from arid to very wet (secondary y-axis on the right). Dotted black line represents the 1971–2000 base**  
 826 **period; the dashed red line connects the 2001–2010 value to the 2041–2070 climate projections for each of the ten models.**  
 827 **The gray shaded area represents the range of model projections. The number in lower left indicates the HLVA vulnerability**  
 828 **index for the metric and location depicted in the associated graph. Note that Oregon, Washington, and Idaho locations are**  
 829 **displayed first in alphabetical order and are followed by those of California, Nevada, and Arizona.**

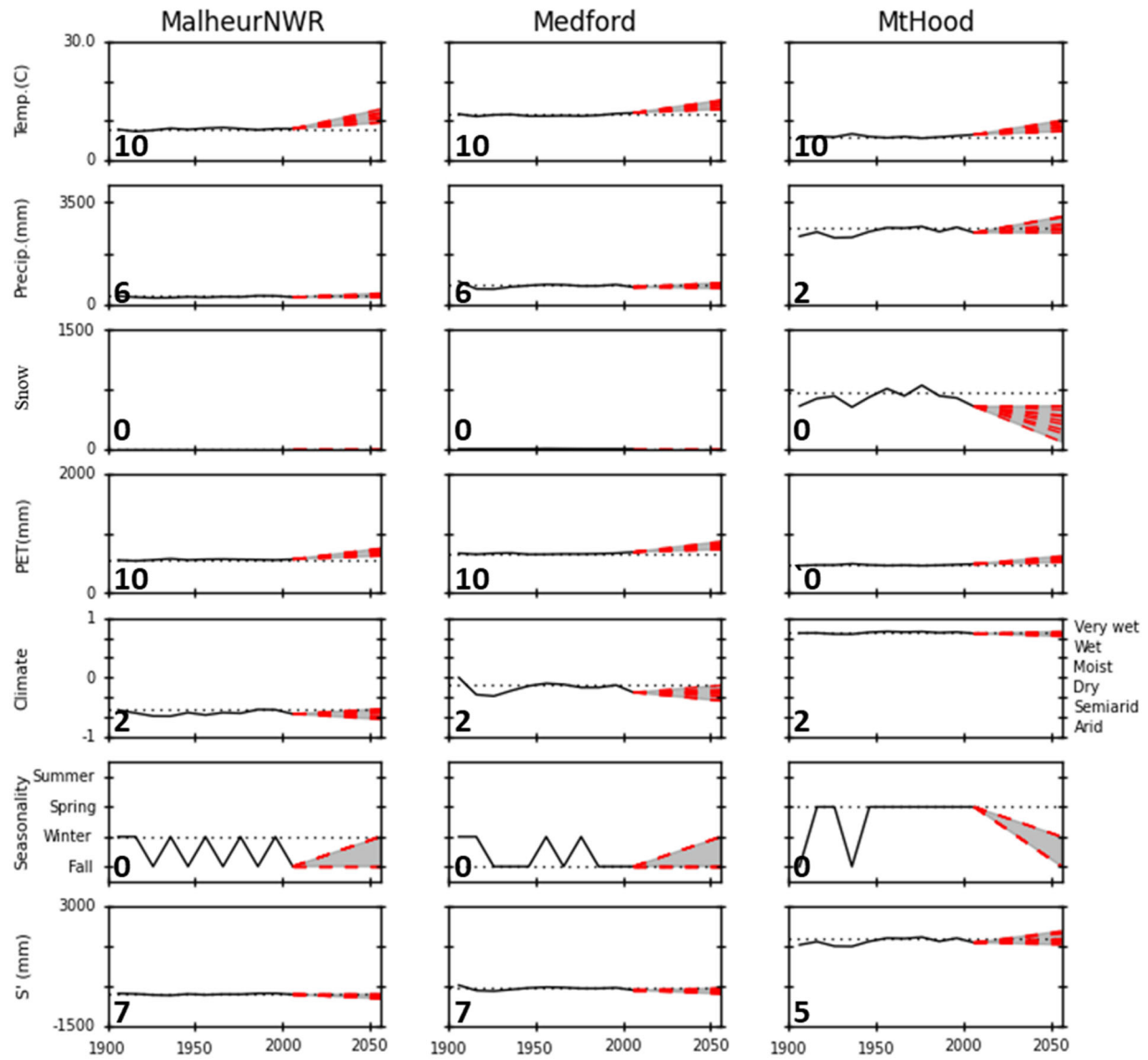


830

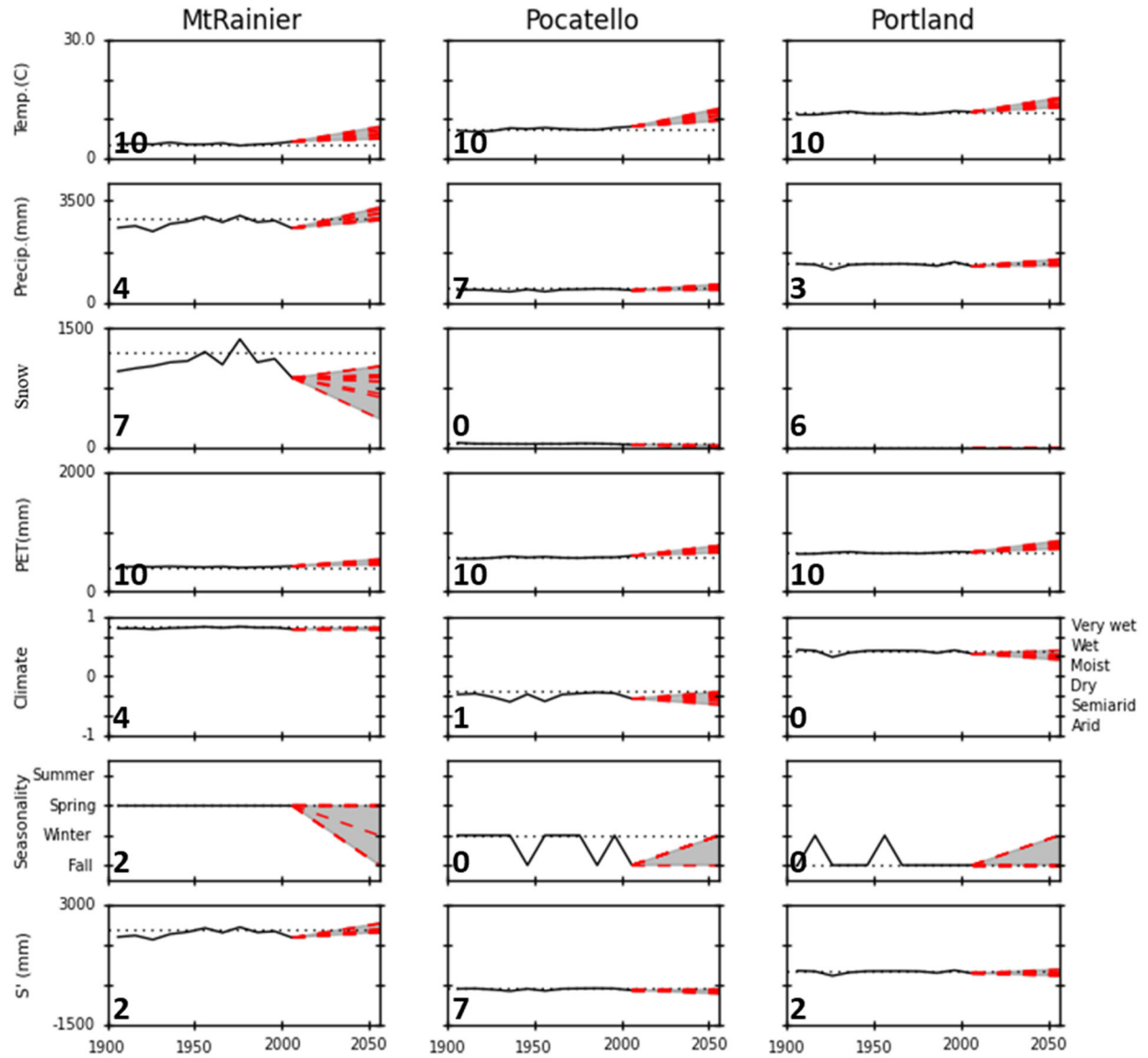


831

832

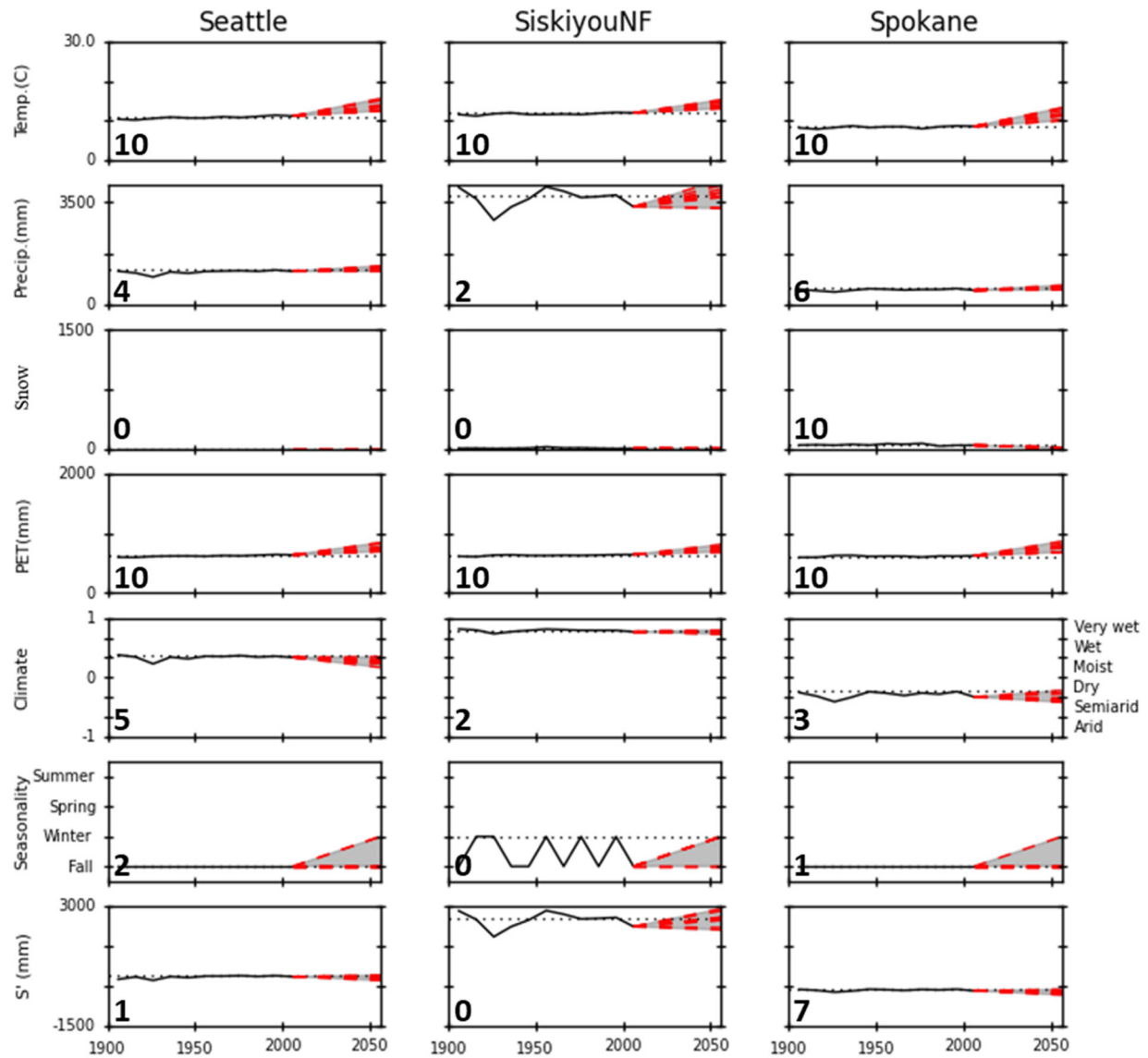


833

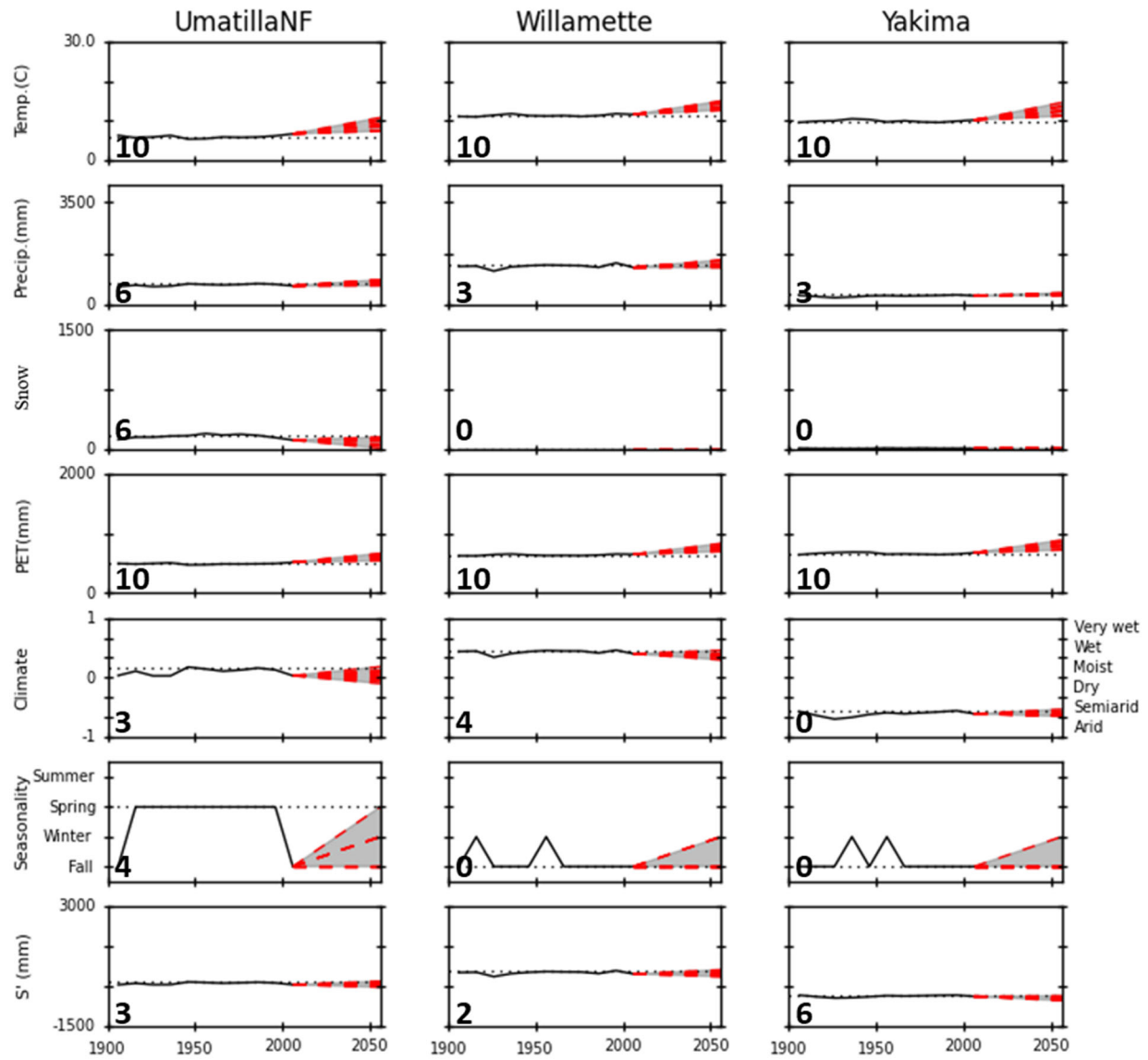


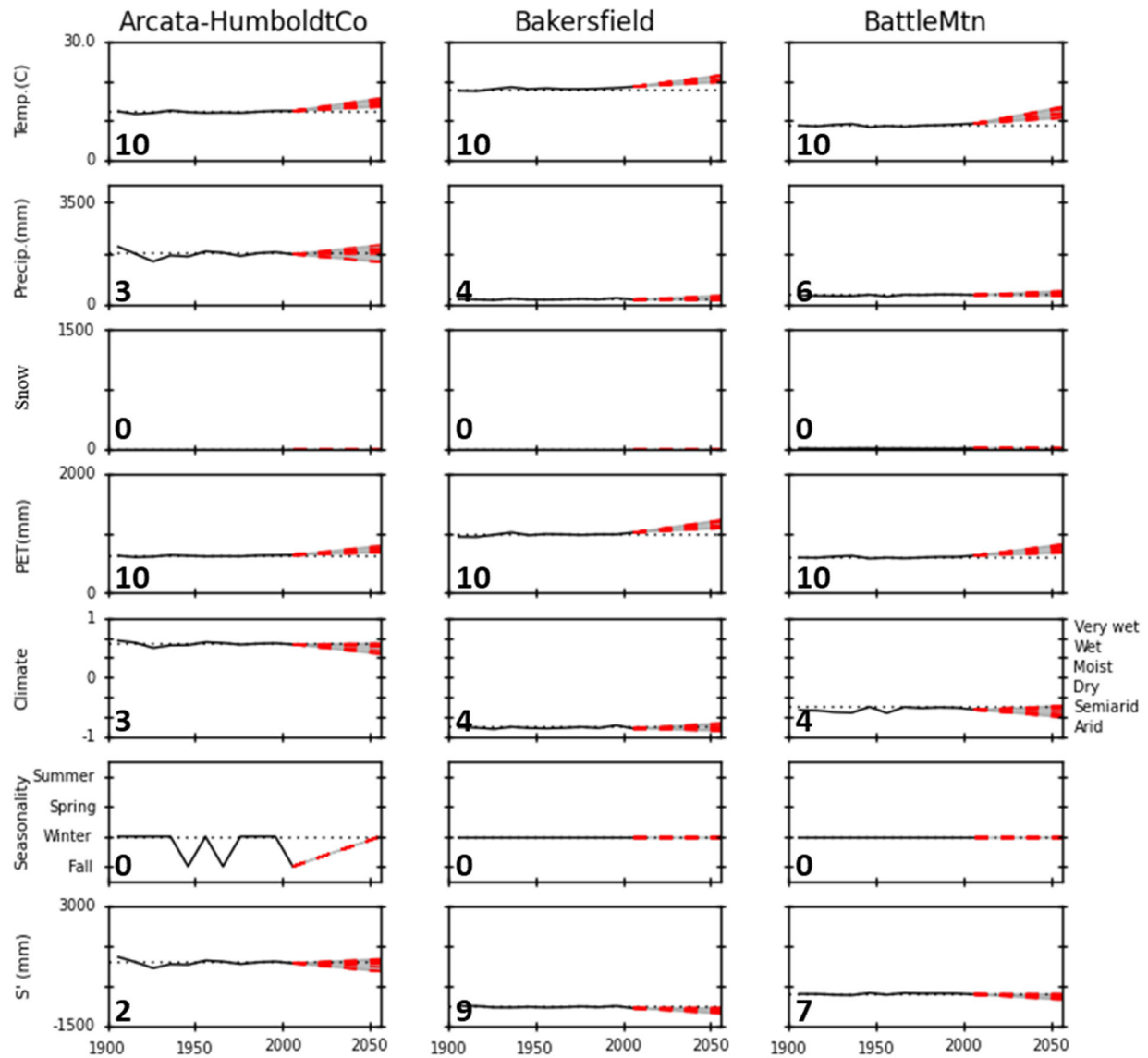
834



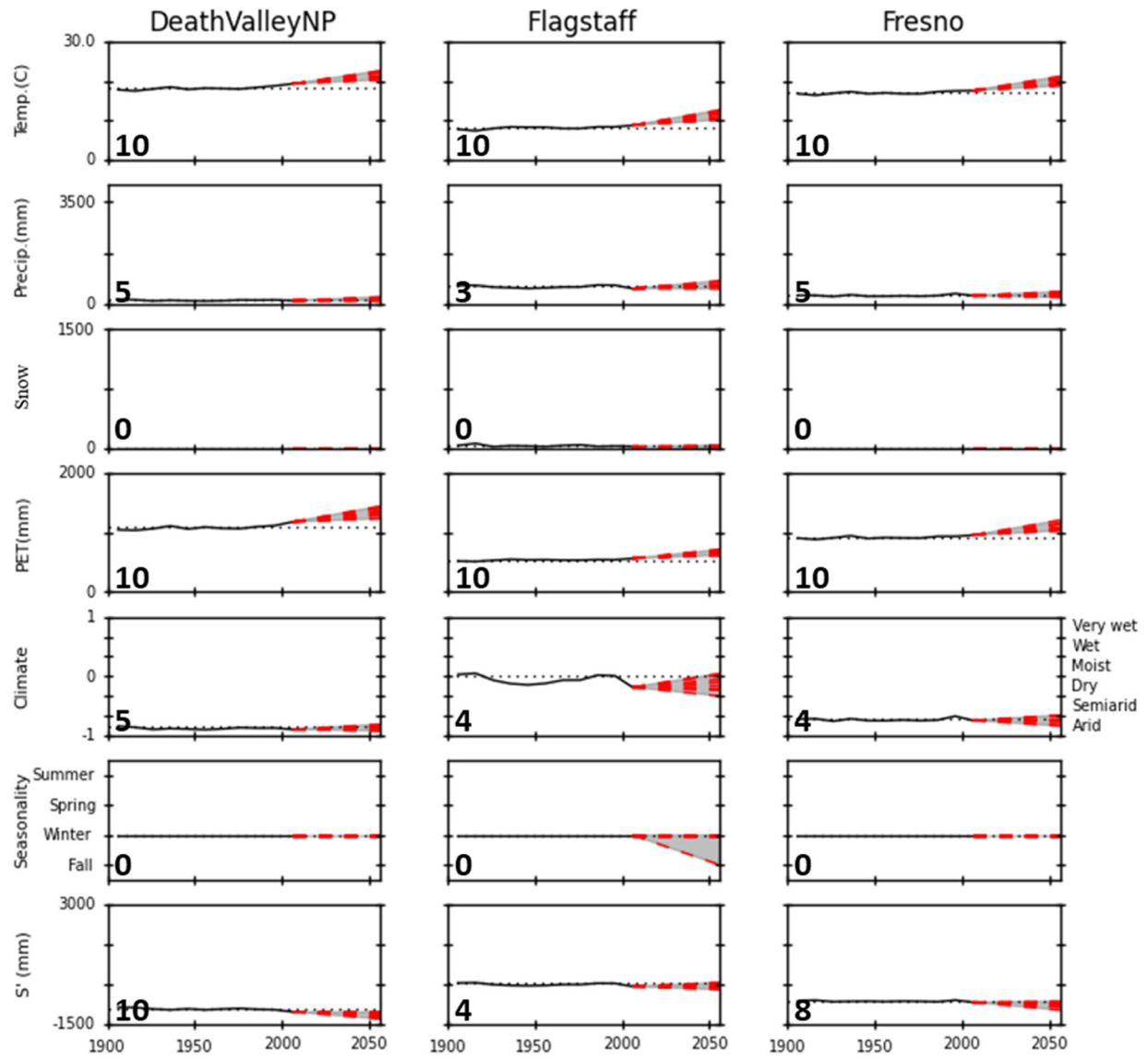


835

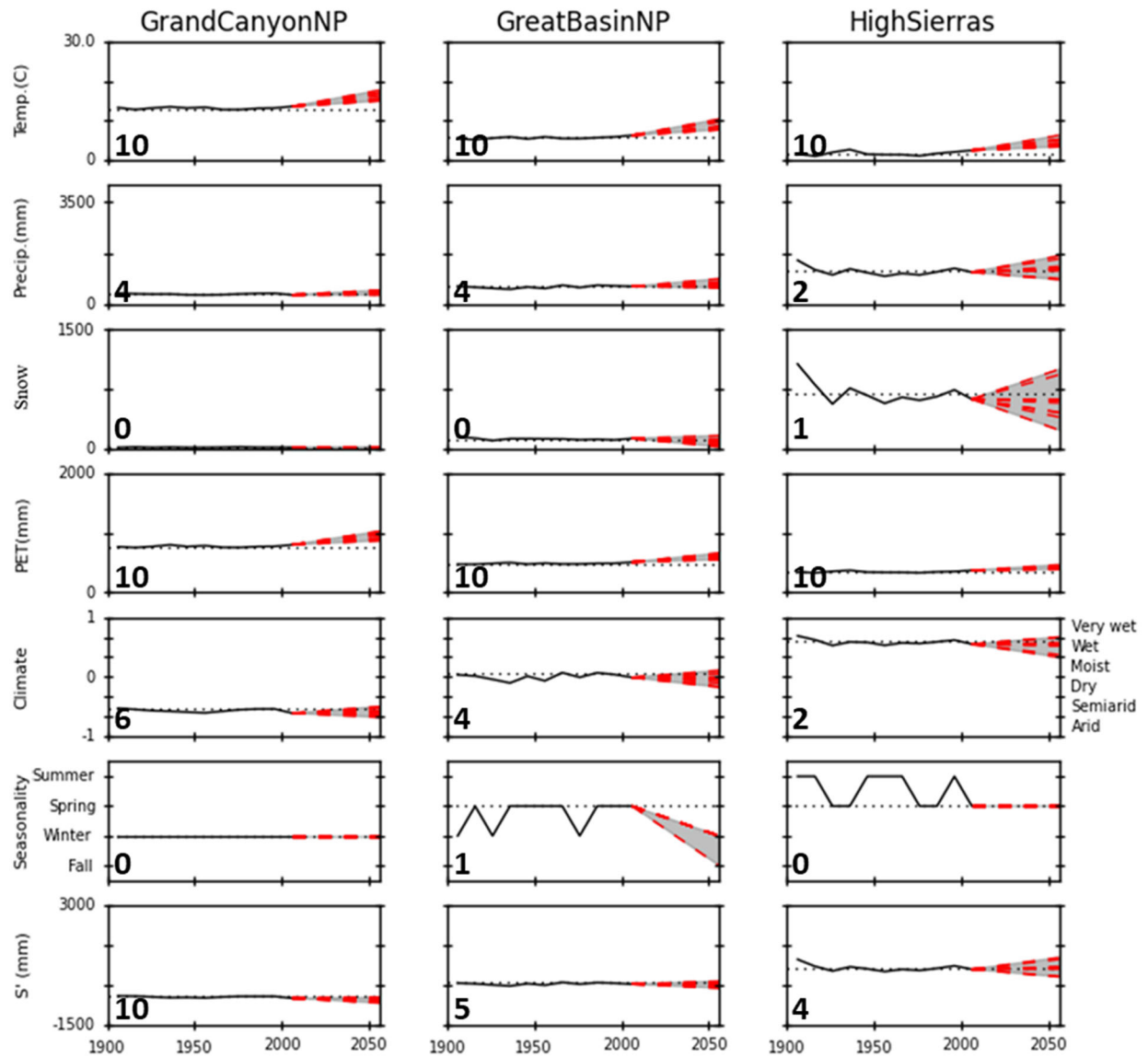


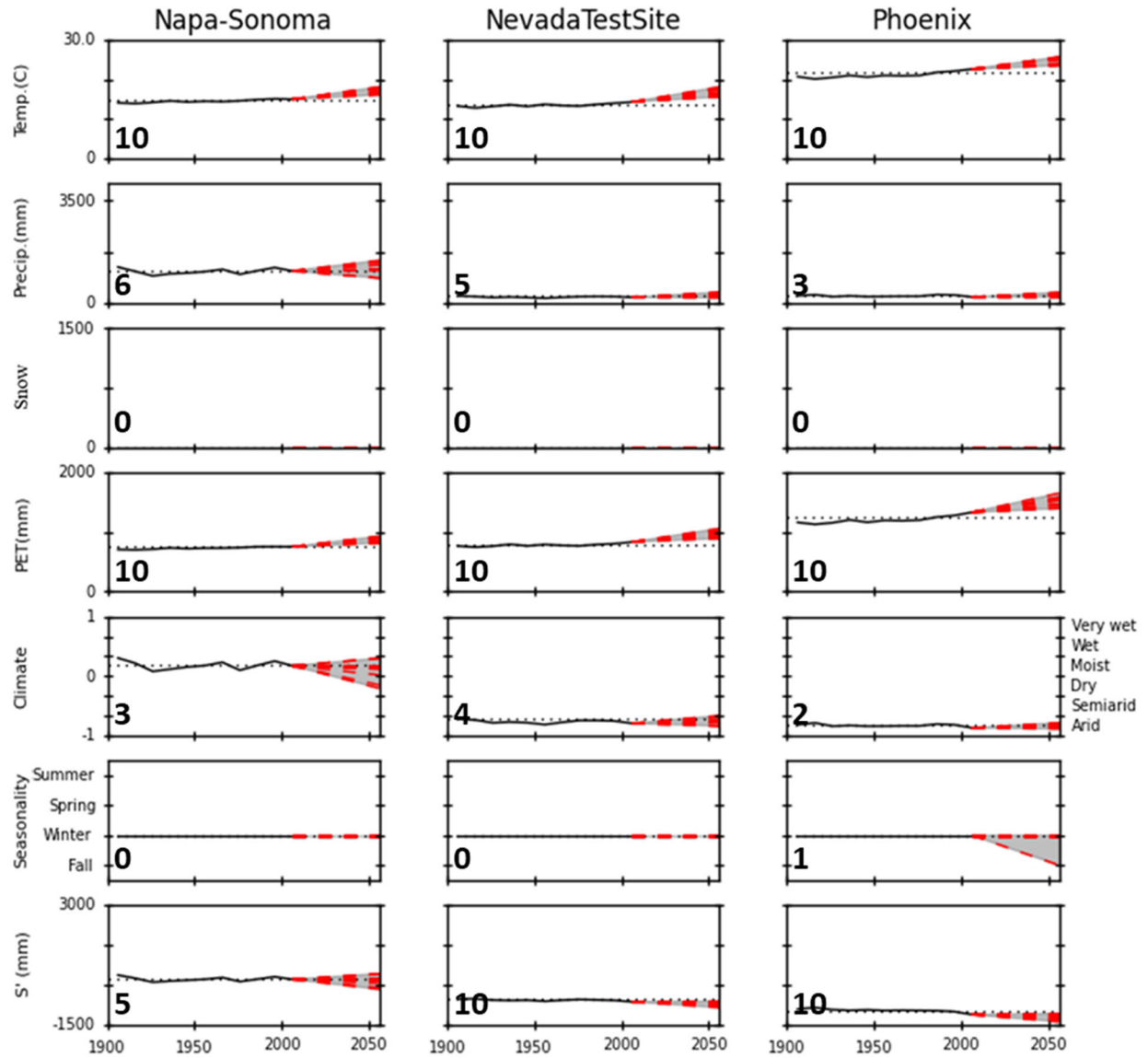


837

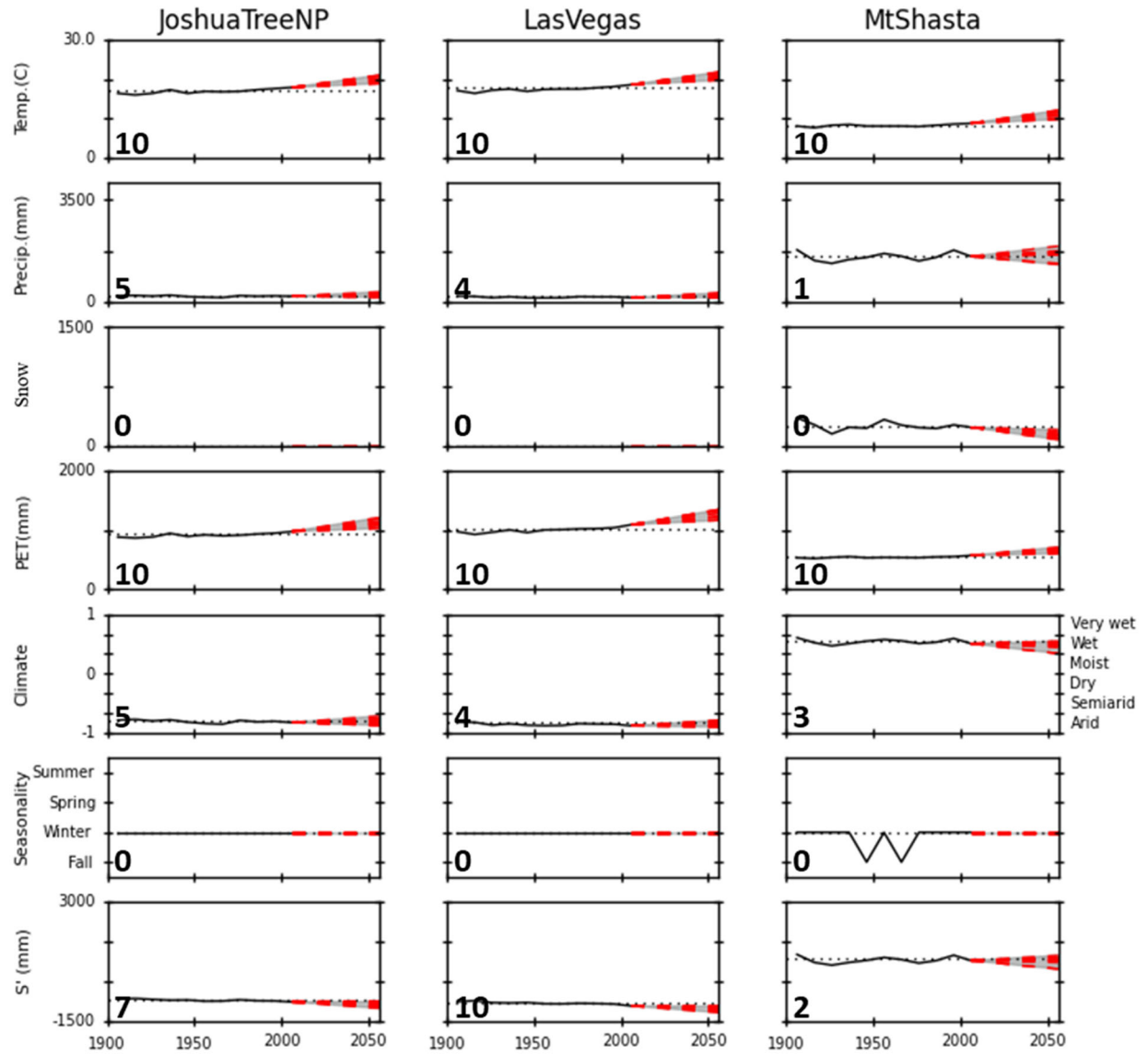


838

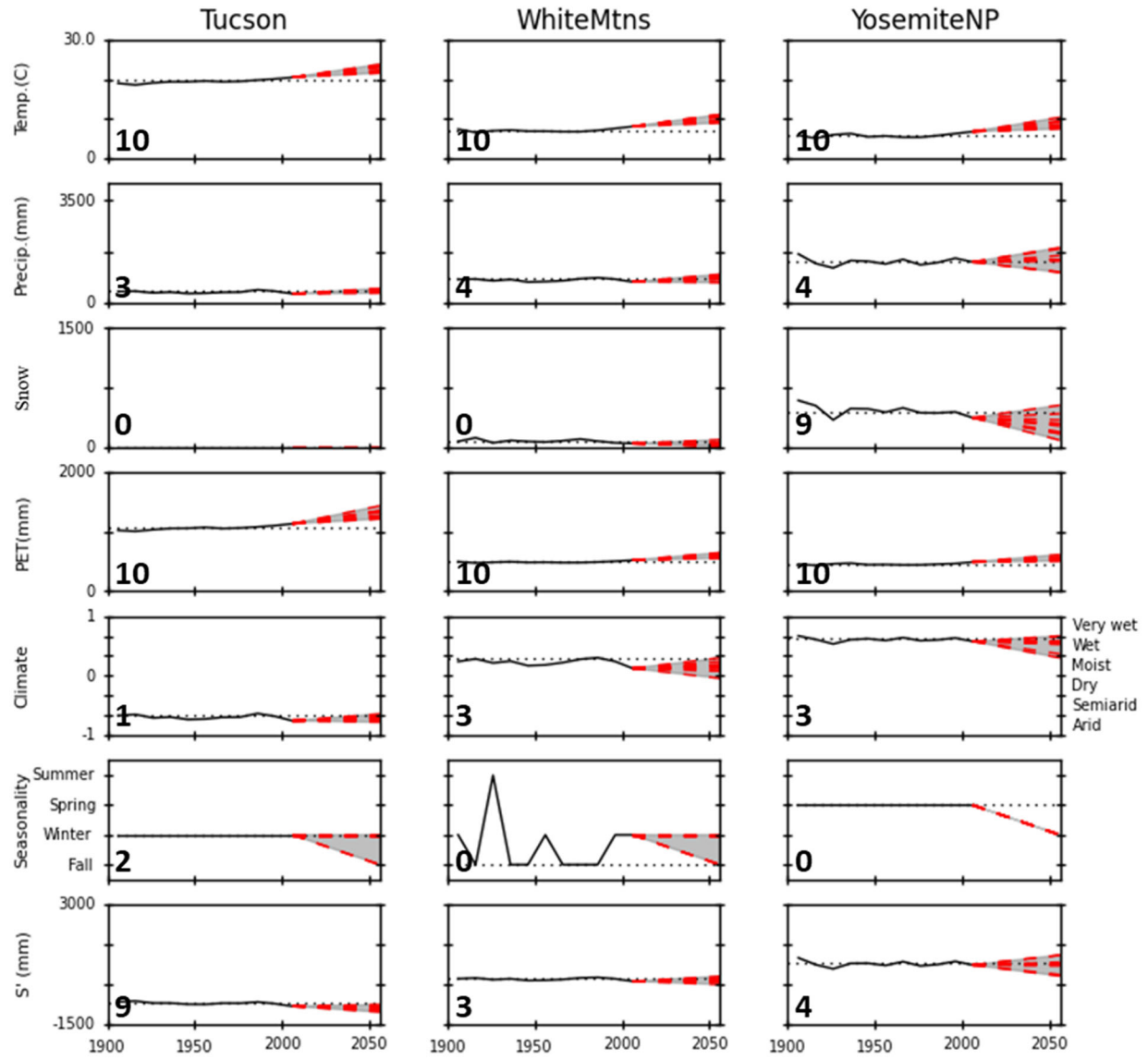




840

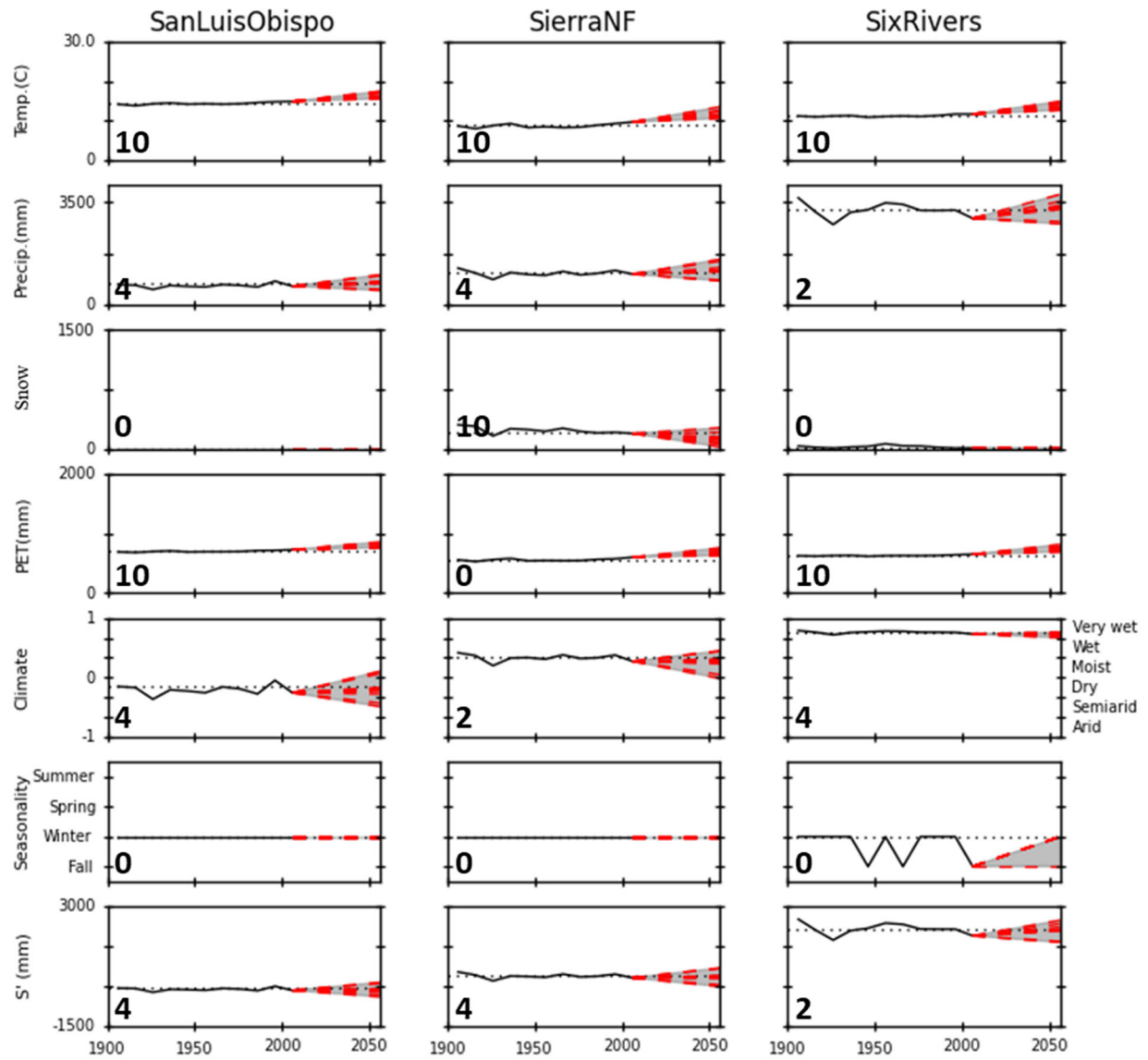


841

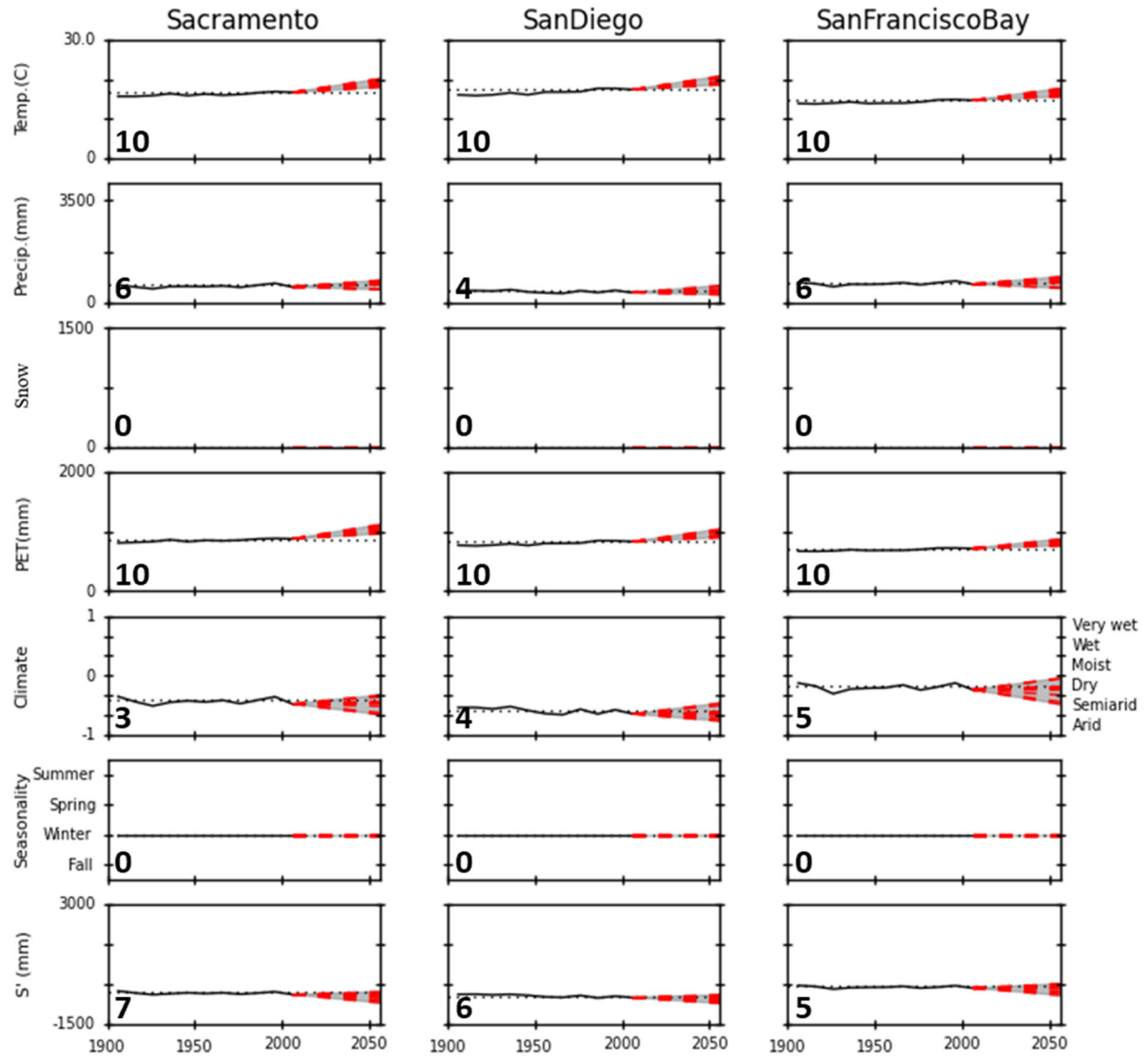


842

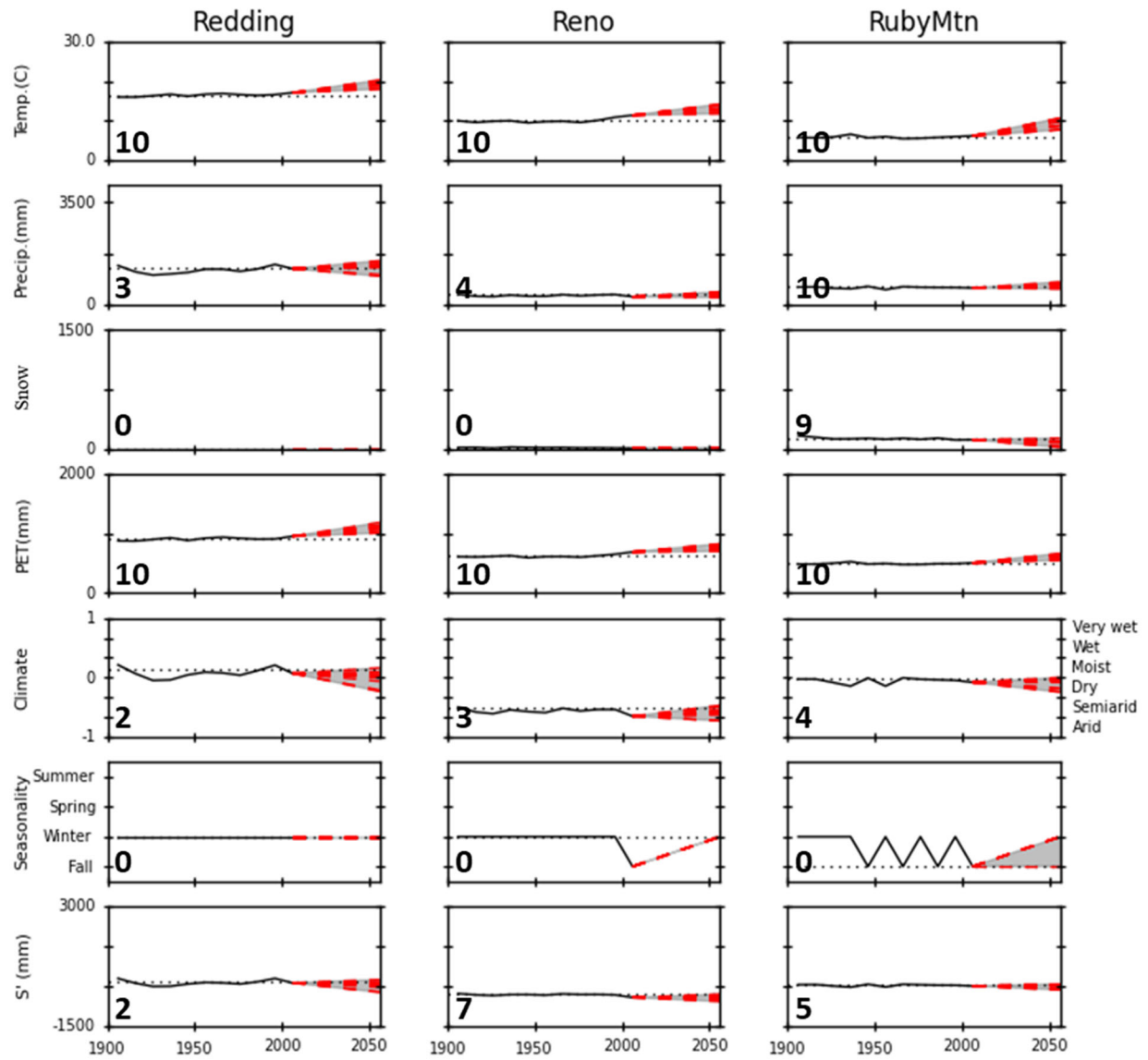




843



844



845